American Society of Hematology
2021 L Street NW, Suite 900,
Washington, DC 20036
Phone: 202-776-0544 | Fax 202-776-0545
editorial@hematology.org

Rapid clonal selection within early hematopoietic cell compartments presages outcome to ivosidenib combination therapy

Tracking no: BLD-2024-027948R2

Sven Turkalj (Dana-Farber Cancer Institute, United States) Felix Radtke (MRC Molecular Haematology Unit, Radcliffe Department of Medicine, Weatherall Institute of Medicine, University of Oxford, United Kingdom) Bilyana Stoilova (MRC Molecular Haematology Unit, Radcliffe Department of Medicine, Weatherall Institute of Medicine, University of Oxford, United Kingdom) Rabea Mecklenbrauck (MRC Molecular Haematology Unit, Radcliffe Department of Medicine, Weatherall Institute of Medicine, University of Oxford, United Kingdom) Angus Groom (MRC Molecular Haematology Unit, Radcliffe Department of Medicine, Weatherall Institute of Medicine, University of Oxford, United Kingdom) Niels Jakobsen (University of Oxford, United Kingdom) Curtis Lachowiez (2The University of Texas MD Anderson Cancer Center, Department of Leukemia, Houston, Texas, USA, United States) Marlen Metzner (MRC Molecular Haematology Unit, Radcliffe Department of Medicine, Weatherall Institute of Medicine, University of Oxford, Oxford, United Kingdom, United Kingdom) Batchimeg Usukhbayar (University of Oxford, United Kingdom) Mirian Salazar (MRC Molecular Haematology Unit, Radcliffe Department of Medicine, Weatherall Institute of Medicine, University of Oxford, United Kingdom) Zhihong Zeng (The University of Texas MD Anderson Cancer Center, United States) Sanam Loghavi (The University of Texas, MD Anderson Cancer Center, United States) Jennifer Marvin-Peek (The University of Texas MD Anderson Cancer Center, United States) Verena Körber (MRC Molecular Haematology Unit, Radcliffe Department of Medicine, Weatherall Institute of Medicine, University of Oxford, United Kingdom) Farhad Ravandi (University of Texas M.D. Anderson Cancer Center, United States) Ghayas Issa (The University of Texas MD Anderson Cancer Center, United States) Tapan Kadia (MD Anderson Cancer Center, United States) Vasiliki Symeonidou (MRC Molecular Haematology Unit, Radcliffe Department of Medicine, Weatherall Institute of Medicine, University of Oxford, United Kingdom) Anne de Groot (MRC Molecular Haematology Unit, Radcliffe Department of Medicine, Weatherall Institute of Medicine, University of Oxford, Oxford, United Kingdom, United Kingdom) Hagop Kantarjian (The University of Texas MD Anderson Cancer Center, United States) Koichi Takahashi (The University of Texas MD Anderson Cancer Center, United States) Marina Konopleva (The University of Texas MD Anderson Cancer Center, Department of Leukemia, Houston, Texas, USA, United States) Courtney DiNardo (The University of Texas MD Anderson Cancer Center, United States) Paresh Vyas (MRC Molecular Haematology Unit, Radcliffe Department of Medicine, Weatherall Institute of Medicine, University of Oxford, United Kingdom)

Abstract:
Acquired resistance to targeted, non-intensive therapies is common in myeloid malignancies. However, the kinetics of selection, the hematopoietic cell compartments where selection occurs, and the molecular mechanisms underlying selection remain open questions. To address this, we studied the kinetics of clonal and transcriptional responses to ivosidenib + venetoclax ± azacitidine combination therapy across hematopoiesis in 8 patients with IDH1-mutant myeloid malignancy. All 8 patients initially responded to treatment but 6 relapsed while 2 remained in sustained remission for >4 years. We performed combined high-sensitivity single-cell (sc) genotyping and scRNA-seq in index-sorted sequential patient samples. In all patients, clonal selection occurred rapidly, within 1-3 treatment cycles. Clonal selection preceded treatment failure by months to years. Relapse was associated with expansion of either clones harboring newly-detected myeloid driver mutations or pre-existing minor clones that underwent differentiation delay upon treatment exposure. In both cases, clonal selection occurred within immature cell populations previously shown to contain leukemic stem cell (LSC) potential. Different genetic alterations within relapse-associated clones converged onto common upregulated transcriptional programs of stemness, branched-chain amino acid catabolism, and genes sensitive to menin inhibition. Importantly, this relapse-associated transcriptional signature was selected within 3 cycles of therapy. In contrast, in both patients remaining in remission, leukemic clones were rapidly eradicated and replaced by clonal and wild-type hematopoiesis. Overall, in patients treated with ivosidenib combination therapy, rapid clonal selection occurs within the first treatment cycles. In those patients destined to relapse, genetically heterogeneous resistant clones are characterized by common transcriptional programs.

Conflict of interest: COI declared - see note

COI notes: C.A. Lachowiez: Consulting/Advisory: AbbVie, Servier, Rigel, Syndax, BMS, COTA healthcare. Research funding: AbbVie; F. Ravandi: Consulting/Advisory: BMS, Syros, AbbVie, Astellas, Prelude. Research funding: Astyex/Taiho, Syros, Amgen, Xencor, Prelude. G. Issa: Consulting/Advisory: Kura Oncology, Syndax, NuProbe, Novartis, AbbVie, Sanofi, AstraZeneca. Research funding: Celgene, Merck, Kura Oncology, Syndax, Astex, NuProbe, Novartis. T. Kadia: Consulting/Advisory: AbbVie, Genentech, BMS, Servier, Sellas, DrenBio. Honoraria: Novartis, Rigel. Research funding: AbbVie, Genentech, BMS, Jazz, Sellas, DrenBio, Regeneron, Amgen, Pfizer, Ascentage, Incyte, ASTEX, AstraZeneca, Cellenkos. H. Kantarjian: Consulting/Advisory/Honoraria: AbbVie, Amgen, Ascentage, Ipsen Biopharmaceuticals, KAHR Medical, Novartis, Pfizer, Shenzhen Target Rx, Stemline, Takeda. M. Konopleva: Consulting/Advisory: AbbVie, AstraZeneca, Auxenion GmbH, Bakx Therapeutics, Boehringer, Dark Blue Therapeutics, F. Hoffmann-LaRoche, Genentech, Gilead, Immune Oncology, Janssen, Legend Biotech, MEI Pharma, Redona, Sanofi Aventis, Sellas, Menarini Group, Vincerx. Research funding: AbbVie, Allogene, AstraZeneca, Genentech, Gilead, ImmunoGen, MEI Pharma, Precision Biosciences, Rafael Pharmaceutical, Sanofi Aventis, Menarini Group. Clinical trials: AbbVie, AstraZeneca, Cellectis, Genentech, Janssen, Pfizer, Sanofi Aventis, Menarini Group. IP: Reata Pharmaceutical. C.D. DiNardo: Consulting/Advisory/Honoraria: AbbVie, AstraZeneca, BMS, Genentech, GenMab, GSK, Immunogen, Notable Labs, Rigel, Schrodinger, Servier, Amgen, Astellas, Gilead, Jazz, Stemline; Research Funding: AbbVie, BMS, Servier, Astex, ImmuneOnc, Cleave, Foghorn, Loxo, Rigel. P. Vyas: Consulting/Advisory: AbbVie, Servier, Rigel, Syndax, AstraZeneca, Debiopharm, Charm Therapeutics. Research funding: Bristol Myers Squibb. Co-founder and Board: Yellowstone Biosciences. SAB: Auron Therapeutics. No disclosures were reported by the other authors.

Preprint server: Yes; bioRxiv https://doi.org/10.1101/2024.12.30.630700

Author contributions and disclosures: S. Turkalj: Data curation, formal analysis, investigation, methodology, visualization, writing-original draft, writing-review & editing. F.A. Radtke: Formal analysis, methodology, visualization, software, writing-original draft, writing-review & editing. B. Stoilova: Conceptualization, data curation, formal analysis, investigation, methodology, writing-review & editing. R. Mecklenbrauck: Data curation, visualization, writing-original draft, writing-review & editing. A. Groom: Investigation, methodology, writing-original draft, writing-review & editing. N.A. Jakobsen: Investigation, methodology, software, writing-review & editing. C.A. Lachowiez: Data curation, writing-review & editing. M. Metzner: Data curation, formal analysis, methodology, writing-review & editing. B. Usukhbayar: Methodology, writing-review & editing. M.A. Salazar: Methodology, writing-review & editing. Z. Zeng: writing-review & editing. S. Loghavi: Data curation, writing-review & editing. J. Marvin-Peek: Data curation, writing-review & editing. V. Körber: Formal analysis, visualization, writing-review & editing. F. Ravandi: Writing-review & editing. G. Issa: Writing-review & editing. T. Kadia: Writing-review & editing. V. Symeonidou: Methodology, writing-review & editing. A.P. de Groot: Methodology, writing-review & editing. H. Kantarjian: Writing-review & editing. K. Takahashi: Resources, writing-review & editing. M. Konopleva: Conceptualization, resources, writing-review & editing. C.D. DiNardo: Conceptualization, resources, writing-review & editing. P. Vyas: Conceptualization, resources, funding acquisition, supervision, project administration, writing-original draft, writing-review & editing.

Non-author contributions and disclosures: No;

Agreement to Share Publication-Related Data and Data Sharing Statement: Bulk targeted NGS, WES, and single-cell genotyping data are available at SRA (https://www.ncbi.nlm.nih.gov/bioproject/PRJNA1139762); accession number: PRJNA1139762. Single-cell RNA-seq data are available at GEO (https://www.ncbi.nlm.nih.gov/geo/query/acc.cgi?acc=GSE273135); accession number: GSE273135. For any additional information/materials, please email the corresponding author, Paresh Vyas. This manuscript reports new basic/translational research data obtained by using samples from patients treated in the clinical trial NCT03471260. The initial clinical data from this trial was published in the following article: Lachowiez CA, Loghavi S, Zeng Z, et al. A Phase Ib/II Study of Ivosidenib with Venetoclax {plus minus} Azacitidine in IDH1-Mutated Myeloid Malignancies. Blood Cancer Discovery. 2023;4(4):276-293.

Clinical trial registration information (if any):

Rapid clonal selection within early hematopoietic cell compartments presages outcome to ivosidenib combination therapy

Running Title: Clonal selection in ivosidenib combination therapy

Sven Turkalj,[1*] Felix A. Radtke,[1*] Bilyana Stoilova,[1*] Rabea Mecklenbrauck,[1*] Angus J. Groom,[1*] Niels Asger Jakobsen,[1] Curtis A. Lachowiez,[2] Marlen Metzner,[1] Batchimeg Usukhbayar,[1] Mirian Angulo Salazar,[1] Zhihong Zeng,[2] Sanam Loghavi,[3] Jennifer Marvin-Peek,[2] Verena Körber,[1] Farhad Ravandi,[2] Ghayas Issa,[2] Tapan Kadia,[2] Vasiliki Symeonidou,[1] Anne P. de Groot,[1] Hagop Kantarjian,[2] Koichi Takahashi,[2] Marina Konopleva,[2] Courtney D. DiNardo,[2] and Paresh Vyas[1,4]

[1]MRC Molecular Haematology Unit, Radcliffe Department of Medicine, Weatherall Institute of Medicine, University of Oxford, Oxford, United Kingdom. [2]The University of Texas MD Anderson Cancer Center, Department of Leukemia, Houston, Texas, USA. [3]The University of Texas MD Anderson Cancer Center, Department of Hematopathology, Houston, Texas, USA. [4]Department of Haematology, Oxford University Hospitals NHS Trust, Oxford, United Kingdom.

*Joint first authors.

ST: Current Address: Department of Pediatric Oncology, Dana-Farber Cancer Institute, Boston Children's Hospital, and Harvard Medical School, Boston, Massachusetts, USA

BS: Current Address: Oxford Vaccine Group, Department of Paediatrics, University of Oxford, Oxford, United Kingdom.

CL: Current Address: Knight Cancer Institute, Oregon Health & Science University, Portland, Oregon, USA.

MK: Current Address: Department of Oncology and Molecular Pharmacology, Albert Einstein College of Medicine, New York, USA.

VS: Current Address: Department of Haematology, Wellcome-MRC Cambridge Stem Cell Institute, University of Cambridge, Cambridge, United Kingdom.

Corresponding author: Paresh Vyas. E-mail: paresh.vyas@imm.ox.ac.uk. Tel: 00 (44)(0)018652 22489.

Text word count: 4400

Abstract word count: 246

Number of Main Figures/Tables: 7

Number of references: 115

Data Sharing Statement: Bulk targeted NGS/WES/single-cell genotyping data are available at SRA (https://www.ncbi.nlm.nih.gov/bioproject/PRJNA1139762); accession number: PRJNA1139762. Single-cell RNA-seq data are available at GEO (https://www.ncbi.nlm.nih.gov/geo/query/acc.cgi?acc=GSE273135); accession number: GSE273135. All other original data is also available. Contact person: paresh.vyas@imm.ox.ac.uk.

Key points

- Ivosidenib, venetoclax ± azacitidine either rapidly selects evolved, resistant leukemic clones or eradicates leukemic clones.
- Resistant clones express RNA signatures of stemness, branched-chain amino acid metabolism, and menin targets.

Abstract

Acquired resistance to targeted, non-intensive therapies is common in myeloid malignancies. However, the kinetics of selection, the hematopoietic cell compartments where selection occurs, and the molecular mechanisms underlying selection remain open questions. To address this, we studied the kinetics of clonal and transcriptional responses to ivosidenib + venetoclax ± azacitidine combination therapy across hematopoiesis in 8 patients with *IDH1*-mutant myeloid malignancy. All 8 patients initially responded to treatment but 6 relapsed while 2 remained in sustained remission for >4 years. We performed combined high-sensitivity single-cell (sc) genotyping and scRNA-seq in index-sorted sequential patient samples. In all patients, clonal selection occurred rapidly, within 1-3 treatment cycles. Clonal selection preceded treatment failure by months to years. Relapse was associated with expansion of either clones harboring newly-detected myeloid driver mutations or pre-existing minor clones that underwent differentiation delay upon treatment exposure. In both cases, clonal selection occurred within immature cell populations previously shown to contain leukemic stem cell (LSC) potential. Different genetic alterations within relapse-associated clones converged onto common upregulated transcriptional programs of stemness, branched-chain amino acid catabolism, and genes sensitive to menin inhibition. Importantly, this relapse-associated transcriptional signature was selected within 3 cycles of therapy. In contrast, in both patients remaining in remission, leukemic clones were rapidly eradicated and replaced by clonal and wild-type hematopoiesis. Overall, in patients treated with ivosidenib combination therapy, rapid clonal selection occurs within the first treatment cycles. In those patients destined to relapse, genetically heterogeneous resistant clones are characterized by common transcriptional programs.

Introduction

Acute myeloid leukemia (AML) is an aggressive malignancy resulting from differentiation delay/arrest and expansion of immature myeloid cells. Two intertwined hierarchies co-exist in AML[1]: a genetic clonal hierarchy, consisting of normal, pre-leukemic, and leukemic clones; and a hematopoietic hierarchy, where cells are arrayed through a continuum of differentiation.[2-9] Whilst pre-leukemic mutations do not usually block differentiation[3-5,10] subsequent genetic and/or epigenetic lesions impair differentiation of hematopoietic

progenitors and/or precursors, enhance self-renewal, and impart functional leukemic stem cell (LSC) properties.[11,12] Different leukemic driver mutations preferentially accumulate at distinct differentiation stages,[5,8,9,12-14] which impacts therapy response.[13,15,16]

Most AML patients[17,18] are ineligible for curative intensive therapies.[19] For this group, options include: venetoclax (VEN) with either azacitidine (AZA; VEN+AZA) or low dose cytarabine.[20-22] For AML with isocitrate dehydrogenase 1 (*IDH1*) mutations,[17,18] the combination of the mutant IDH1 inhibitor ivosidenib (IVO) with AZA is also established.[23] Although these non-intensive approaches commonly produce an initial response, relapse typically occurs.

Distinct and shared genetic mechanisms of resistance to VEN+AZA and IVO were proposed.[24] Shared mechanisms include mutations in genes encoding signaling molecules (e.g. *FLT3* and *RAS), TP53* mutations, and complex karyotype.[25-27] Distinct mechanisms include mutations in genes regulating apoptosis (e.g. *BAX*) in VEN-treated patients[28] and *IDH2* mutations in IVO-treated patients[26]. VEN or VEN+AZA resistance was also attributed to higher BCL-xL and MCL-1 protein expression,[29] FLT3 and RAS signaling,[27,30,31] reduced mitochondrial priming,[32] increased non-glycolytic catabolism and oxidative phosphorylation (OxPhos),[33-35] and monocytic differentiation.[36] Conversely, transcriptional signatures of stemness correlate with resistance to mutant IDH inhibition.[37,38]

To evaluate VEN and IVO-containing regimens for *IDH1*-mutant myeloid malignancy, we conducted a phase Ib/II study of IVO+VEN±AZA[39] (NCT03471260). The initial overall response rate (ORR) in 31 patients was 94%. In 6/9 patients with available samples who relapsed after an initial response, relapse was associated with genetic evolution.[39] Selected mutations occurred in genes encoding transcription factors and signaling molecules. However, open questions included the clonal and cellular basis of therapy-induced selection, the kinetics of selection, and the transcriptional basis of resistance. Furthermore, some patients remained in remission for >4 years without allogeneic hematopoietic stem cell transplantation (alloHCT), raising questions about the nature of their clonal response.

To address this, we studied 8 IVO+VEN±AZA-treated patients where initial morphologic blast clearance was achieved and sequential bone marrow (BM) samples were available. With longer follow-up, 6/8 patients relapsed while 2 remained in remission for 48 and 57 months. Using sequential samples, we performed high-fidelity single-cell (sc) genotyping coupled with immunophenotypic and scRNA-seq analysis,[10,40] to investigate longitudinal dynamics of clonal response through hematopoiesis and transcriptional features of relapse.

Methods

Patients and sample processing

BM samples were collected with informed consent either on trial (NCT03471260 trial) or from age-/sex-matched individuals, with no hematologic malignancy (MARCH study (17/YH/0382)[10]). Sample were processed as described.[10,39]

Outcome parameters

Remission was defined according to 2022 ELN.[19] Overall survival (OS) was defined from first day of therapy to death or last follow-up. Duration of response (DOR) was defined from the first documented therapy response (MLFS/PR/CRi/CR) to treatment failure. Treatment failure was defined as relapse or disease progression.

Bulk DNA sequencing

Details are in supplemental Methods. An 81-gene targeted Next Generation Sequencing (NGS) panel (supplemental Table 1) was performed;[39] a 97-gene targeted NGS panel[10] (supplemental Table 1) was additionally performed for patients 4/9. Whole-exome sequencing (WES) was performed on patients 4/5/10/11 at baseline and 11/14 at relapse, using $CD45^{dim}$ blasts and $CD3^{+}$ T control cells.

Cytogenetic analysis and molecular MRD assessment

Conventional karyotyping was performed.[39] *IDH1* mutation was assessed by Sanger sequencing (10–20% sensitivity) and by NGS (1–2% sensitivity). Measurable residual disease (MRD) was assessed by flow cytometry (0.1-0.01% sensitivity).

Flow cytometry and FACS

FACS staining[10] (supplemental Methods) was performed with antibodies against CD38/CD10/CD117/CD45RA/CD123/CD90/CD34/lineage marker cocktail (CD2/CD3/CD4/CD8a/CD19/CD20/CD235), and 7-AAD. FACS analysis and single-cell FACS-sorting were performed. Single-cell index data was collected. Cells from the NOC156 control sample were sorted onto ~10% of each plate. Flow cytometry data analysis on non-pre-enriched samples was performed using FlowJo v10.8.1 and R (v4.3.1).

TARGET-seq+

Procedures[10,41] are in supplemental Methods. Transcriptome libraries were sequenced at 1 million reads/cell (except pt5, sequenced at 40,000 reads/cell). Genotyping libraries were sequenced at 2,000 reads/amplicon/cell.

Single-cell genotyping analysis

Details are in supplemental Methods. Briefly, mutant and WT reads at each locus were computed using TARGET-seq,[40] getITD,[42] and custom pipelines. After filtering based on coverage, single-cell mutation calling was performed using single-cell variant allele

frequency (scVAF). ScVAF and mutant read thresholds were established by genotyping WT control BM cells.[1,10,43] Single-cell copy number alterations (CNAs) were inferred from RNA. RNA reads were pre-processed with a custom pipeline.[10] Quality filtering and normalization, performed using Seurat (v5.0.1),[44] SingleCellExperiment (v1.24.0),[45] and inferCNV(v1.18.1),[46] were followed by custom CNA calling. Single-cell mutation and CNA calls were merged. infSCITE[47] was used to determine the most likely phylogenetic tree. After correction for allele drop-out, co-occurrence of somatic events was used to assign each cell to a clone. Finally, each cell was assigned to an immunophenotypic population using surface markers.

For patients 4/5/9/10/11/14/18, the size of each clone within live, lineage-negative (Lin^-) cells at each time point was inferred, taking the population size and respective clone sizes into consideration.

Transcriptome analysis

Details are in supplemental Methods. Briefly, clone-specific differential expression analysis was performed using MAST.[48] Transcriptional similarity was evaluated using a correlation matrix interrogating the overlap of dysregulated genes across patients. Regulon analysis was performed using pySCENIC (v0.12.1[49]) and AUCell (v1.30.1).[50] An *IDH*-R132H signature was derived from public bulk RNA-seq data[51] using Limma-voom.[52] The relapse signature was determined by Fisher's combined probability test.[53] Gene Set Enrichment Analysis (GSEA) was performed using the molecular signature database genesets.[54,55] Additionally, the *IDH*-R132H signature, public hematopoietic, LSC, and menin-related signatures,[8,12,56-72] and a manually curated HSC/LSC self-renewal signature, were probed (supplemental Table 5A-5B). GSEA and single-cell activity of gene sets was performed using fgsea[73] and AUCell.[50]

Quantification and statistical analysis

Statistical data analysis was performed using R (v4.3.1). Plots were generated using ggplot2 (v3.3.6) or FlowJo (v10.8.1). Statistical tests and summary statistics are in each figure legend.

Results

Patient cohort and experimental strategy.

8 patients (pts) treated with IVO+VEN±AZA were studied (Figure 1A; Table 1). Pts 11/5/20/14 were newly diagnosed, whereas pts 9/4/18/10 had relapsed disease. Treatment was: VEN days 1–14; IVO 500 mg continuously, beginning on cycle (C) 1 day 15; and, in pts 18/20, AZA 75mg/m^2 for 7 days was also administered. pt20 received IVO+VEN+AZA for

two cycles, followed by IVO monotherapy, after experiencing prolonged cytopenia in C1–2. After a median follow-up of 40.3 months (data cut-off 2023-12-14), median DOR was 18.5 months, median time on treatment was 20.3 months, and median OS was 45.5 months; pts 18/10 remained on treatment.

Figure 1B illustrates our approach. We established the sizes of immunophenotypic normal BM mononuclear cell (BMMNC) lineage-negative (Lin^-) compartments in 10 normal human BM samples (supplemental Figure 1A; supplemental Table 2A). We defined the sizes of the Lin^-CD34^+ hematopoietic stem and progenitor cell (HSPC), $Lin^-CD34^-CD117^+$ granulocyte-macrophage (GM) precursor, and $Lin^-CD34^-CD117^-$ mature myeloid cell compartments. We then analyzed these compartments in patient samples (supplemental Figures 1B–1D; supplemental Table 2B).

Next, we index-sorted single cells from these compartments from: (a) baseline; (b) early response; and (c) either treatment failure or long-term remission. Single-cell genotype, immunophenotype, and transcriptome were obtained. Clonal identities of single cells were assigned using patient-specific mutational panels (supplemental Tables 3A–3D) and CNA inference from scRNA-seq (supplemental Tables 3E-3G). 14,383 single cells were assigned to clones. Finally, we integrated clonal status, immunophenotype, and transcriptome for each cell.

Rapid selection of newly-detected resistant clones occurs within small immature BM populations, months or years prior to treatment failure.

In 6 relapsing patients, the time from initial response to relapse varied from 3 months (pt11) to ~4 years (pt5). We identified 2 clonal selection patterns. Pts 11/5/20 relapsed with clones undetected prior to treatment; conversely, in pts 14/9/4, minor clones, detected at trial entry, expanded upon therapy exposure. We first report on patients with newly-detected clones.

Pt11 (*de novo* AML) had a DOR of 3.4 months on IVO/VEN. Relapse was associated with a genetically evolved clone, not detected at baseline but selected already by end of cycle 3 (EOC3). Pre-treatment, *DNMT3A* (D), *NPM1* (N), *IDH1* (I), and *NRAS* (Nr) mutations were detected (Figures 2A-2B; supplemental Figures 2A–2B). Single-cell analysis revealed two dominant clones at baseline, DNI and DNINr (Figure 2B; supplemental Table 4A). These dominated the GM precursor compartment (most expanded population) but were also detected within lymphoid-primed multipotent progenitors (LMPP) and granulocyte-monocyte progenitors (GMP; Figure 2C). Though we have not functionally tested LSC capacity in these samples, all three compartments were previously shown to contain LSC potential.[11,12] By EOC3, the patient had achieved CR, with the BM largely composed of wild type (WT) mature myeloid cells; however, we also detected a genetically evolved clone harboring an additional

FLT3-ITD (F) mutation (DNINrF clone). By EOC3, the DNINrF clone comprised ~90% of the small-sized LMPP, GMP, and GM precursor BM compartments (Figures 2A–2C). At EOC3, compared to WT precursors, DNINrF precursors were transcriptionally enriched for RAS/MAPK/KIT signalling pathways and HSC/LSC signatures, possibly accounting for impaired differentiation (supplemental Figure 2C). The DNINrF clone led to rapid relapse post-C3.

In 2 other patients (pts 5/20), newly-detected clones were also selected early but treatment failure ensued with slower kinetics. Pre-treatment, pt5 (*de novo* AML) had del(5)(q22q35) (-5q) and *RUNX1* (R), *ASXL1* (A), *IDH1* (I), and *TET2* (T) mutations (Figures 2D–2E; supplemental Figures 3A–3D). The (-5q)RAI clone, dominant at baseline, was eradicated by EOC3 (Figures 2D–2E; supplemental Table 4B), when the patient was in CR and mature myeloid cells were mainly WT. However, at EOC3, the ancestral (-5q) clone persisted in ~1% of all BM Lin^- cells. Moreover, a previously undetected *SF3B1*-K700E-mutant clone ((-5q)S) was present in < 0.1% of BM Lin^- cells (Figures 2D–2E). Interestingly, despite its small size at EOC3, the (-5q)S clone was detected in 4/12 of immunophenotypic hematopoietic stem cells (HSCs; Figure 2F). In parallel, an independent *TET2*-mutated clone (T), detected at baseline, also persisted. By EOC11, when the patient was still in CR, all 3 clones ((-5q), (-5q)S, and T) had expanded. However, whereas the T clone differentiated efficiently, (-5q) and (-5q)S clones were dominant within HSCs (70% of HSC) and megakaryocyte-erythroid progenitors (MEP; 56% of MEP; Figure 2F). Pt5 was MRD-negative at EOC3 and EOC11 (IVO/VEN response: 47.5 months, supplemental Table 1I). 40 months after EOC11, pt5 progressed to myelodysplasia (MDS) with the (-5q)S clone (supplemental Tables 1A and 1F); lenalidomide monotherapy was initiated.

Pt20 (*de novo* AML) had a DOR of 24.3 months. Pre-treatment, two *TET2* (T), and *ASXL1* (A), *SRSF2* (S), *IDH1* (I), and *BRAF* (B) mutations were detected within a complex clonal structure (supplemental Figures 4A–4C). The TTASI clone, dominant pre-treatment, was eradicated by EOC1 (BM blast reduction from 79% to 6%) and replaced by hematopoiesis from earlier clones (TTA/TTAB/TTAS; supplemental Figures 4C–4D). In parallel, a newly-detected *RUNX1*-Y414fs*186 (R) mutation was selected within a minor TTASR clone in the small-sized common myeloid progenitor (CMP) compartment, previously shown to have LSC potential in AML.[74] By EOC11, when the patient was in morphological leukemia-free state (MLFS), the TTASR/TTAS clones had expanded in the CMP/MEP/GM precursor compartments, whereas TTAB/TTA/TT clones were more prominent in mature myeloid cells (supplemental Figure 4D). 15 months later, the expansion of a primitive myeloid population gave rise to AML with the *RUNX1*-Y414fs* mutation (69% VAF in BMMNCs; supplemental Table 1F),[39] suggesting defective differentiation of the TTASR clone led to treatment failure.

Although pt20 remained MRD-positive, the dynamics of leukaemia-associated immunophenotypes (LAIP) did not reflect the kinetics of an expanding clone (supplemental Table 1I).

Overall, in all 3 patients, therapy-resistant clones, undetected prior to therapy, were selected within 1–3 treatment cycles and expanded within small-sized immature populations. Clonal selection occurred months or years prior to treatment failure.

Minor pre-existing clones expand under therapeutic pressure within immature BM populations, months prior to relapse.

In 3 other patients, therapy resistance arose from complex clonal adaptation to treatment.

In pt14 (*de novo* AML), *DNMT3A* (D), *NPM1* (N), and *IDH1* (I) mutations, and trisomy 4 (+4), were detected at baseline (Figures 3A–3B; supplemental Figures 5A–5D). Pt14 was treated with IVO/VEN and responded for 6.7 months. At baseline, the DNI clone was dominant (Figure 3B; supplemental Table 4C), whereas the DN(+4) clone was detected at similarly low levels in multipotent progenitors (MPP), GM precursors, and mature myeloid cells (Figure 3C). By EOC3 (CR), the DNI clone was nearly eradicated, and hematopoiesis was largely WT (Figures 3B–3C). However, the DN(+4) clone was now detectable within LMPPs and dominated specifically the GM precursor compartment, despite the precursor population being small-sized (Figure 3C). Despite its clonal dominance within precursors, the DN(+4) clone contributed minimally to mature myeloid cells, suggesting abnormal differentiation (Figure 3C). At EOC3, compared to WT precursors, DN(+4) precursors upregulated HSC/LSC/LMPP, pro-proliferative, and branched-chain amino acid (BCAA) catabolism transcriptional signatures; conversely, they downregulated myeloid maturation and inflammatory signatures, reflecting impaired differentiation (supplemental Figures 5E–5F). Interestingly, HSC/LSC/LMPP signatures were upregulated in DN(+4) precursors at EOC3 compared to baseline, suggesting transcriptional adaption of this clone (supplemental Figure 5G). 6 months following EOC3, at relapse, the DN(+4) clone dominated LMPPs and was still the major contributor to expanded GM precursors. Although the DN(+4) clone was detected in mature myeloid cells, its frequency was higher in immature versus mature myeloid cells (supplemental Figure 5H). Though two smaller clones evolved from DN(+4) with trisomy 20 or 21, the dominant clone at relapse was DN(+4).

Pt9 had relapsed after decitabine treatment and responded to IVO/VEN for 3.9 months. At baseline, pt9 had *ASXL1* (A), *IDH1* (I), *STAG2* (S), and *FLT3* tyrosine kinase domain (*FLT3*-TKD, F) mutations, del(5)(q22q33) (-5q), and trisomy 11 (+11; Figures 3D–3E; supplemental Figures 6A–6D). Pre-treatment, AIS and AI(-5q+11) clones were dominant (Figure 3E; supplemental Table 4D) in different BM compartments (Figure 3F). A smaller *FLT3*-TKD-

mutated AISF clone was present within GM precursors and differentiated into mature myeloid cells (Figure 3F). By EOC3, when the patient was in CR, 73% of mature myeloid cells were either WT or harbored a single *ASXL1* mutation. However, the minuscule AISF clone gained advantage specifically within small-sized LMPP/GMP compartments, as opposed to mature myeloid cells (Figure 3F). Relapse ensued months later, with expansion of GMPs and, to a lesser extent, LMPPs/GM precursors. All 3 populations were dominated by the AISF clone (Figure 3F). In fact, the ratio of this clone in immature versus mature cells increased at relapse compared to baseline (supplemental Figure 6E), suggesting impaired differentiation. Accordingly, compared to AISF precursors at diagnosis, AISF precursors at relapse upregulated pro-proliferative and LSC/HSC signatures, while downregulating myeloid differentiation signatures (supplemental Figure 6F-G). Of note, 2 *CEBPA* and 1 *RUNX1* mutation (12–22% VAF) were detected by bulk NGS at relapse (supplemental Table 1F); we were technically unable to genotype these loci, limiting clonal hierarchy dissection.

Complex polyclonal dynamics were observed in pt4 (supplemental Figure 7), the only patient with antecedent MDS/MPN, who was treated with IVO/VEN having failed both AZA and olutasidenib treatments. At baseline, the expanded CMP compartment was dominated by a clone with *SRSF2* (S), *IDH1* (I), *ASXL2* (A), and *JAK2* (J) mutations (SIAJ clone) (supplemental Figure 7A-G). Although this clone persisted through treatment, it was reduced compared to baseline (supplemental Figures 7F-7G). Conversely, two clones harboring CNAs (SIA(-20q-7) and SIA(-20q+1)), both minor at baseline, expanded by EOC3 (supplemental Figure 7G-H). Relapse was highly polyclonal, with multiple clones that did not mature efficiently (supplemental Figures 7G–7H).

In summary, minor, pre-existing clones can also be selected within 1-3 therapy cycles. While differentiating at diagnosis, these clones rapidly gain advantage upon treatment exposure, specifically within populations previously shown to contain LSC potential.

Transcriptional signatures of stemness, non-glycolytic catabolism, and menin targets are upregulated across resistant clones by EOC3.

Although clonal selection was rapid in all patients analysed above, a unifying genetic signature of relapse was not identified. This led us to investigate whether relapse-associated clones (RACs) had shared transcriptional signatures, arising due to either genetic evolution or putative non-genetic adaptation. We leveraged transcriptomic data from 9,006/10,117 cells passing QC from 4 patients (pts 11/9/14/4) where high-quality scRNA-seq was available from baseline/EOC3/relapse (supplemental Figures 8 and 9A). We analysed transcriptional differences between clones dominant at baseline versus relapse, within the same cell populations expanded at baseline and relapse (Figure 4A, supplemental Figure

9A, supplemental Table 5C), thus avoiding transcriptional differences being driven by differentiation stage. This revealed a substantial overlap in relapse signatures between pts 11/9/14 but not pt4 (supplemental Figures 9B-9C), suggesting resistance mechanisms in pt4 (only patient with an MDS/MPN diagnosis and an *SRSF2* mutation) and pts 11/9/14 (AML diagnosis) were distinct. We hereafter focused on pts11/9/14.

Interestingly, genes downregulated by *IDH1*-R132H mutations in primary human HSPCs (*IDH1*-R132H DOWN signature)[51] were upregulated at relapse (Figure 4B and supplemental Figures 9D-9E). Notably, RACs in pts 11/9 were *IDH1*-mutant. Strikingly, of over 22,000 signatures, the *IDH1*-R132H DOWN signature was consistently among the most upregulated. This suggested that: (a) IVO was on target at relapse; (b) resistant clones bypass the transcriptional consequences of *IDH1* mutations.

Next, we asked whether pathways associated with VEN resistance were transcriptionally enriched at relapse (Figure 4C). OxPhos and non-glycolytic catabolic pathways, such as fatty acid oxidation, the TCA cycle, and amino acid metabolism, were enriched at relapse. Nucleotide biosynthesis was also upregulated. All these processes contribute to VEN resistance.[33-35,75] RACs also upregulated pro-proliferative and DNA repair pathways (supplemental Figure 9F).

Given that LSCs rely on OxPhos,[76] increased OxPhos signatures at relapse suggested increased stemness within RACs. Indeed, RACs across pts 11/14/9 were enriched for LSC/HSC signatures and depleted for myeloid differentiation signatures (Figure 4D). Notably, the transcriptional increase in stemness is associated with resistance to mutant IDH inhibition.[37,38] Genes promoting LSC function, like *INPP4B/SOCS2/MYB/MEIS1/MEF2C/PBX3/HOXA/HOXB*,[77-86] as well as HSC self-renewal, like *MLLT3/ERG/GATA2/ETV6/MSI2*,[87-91] were upregulated within RACs (Figure 4E). *BCAT1/2*, encoding BCAA-catabolizing enzymes overexpressed in LSCs,[92-94] were also upregulated. Accordingly, BCAA catabolism was transcriptionally upregulated (supplemental Figure 9G). Conversely, inflammatory pathways were depleted within RACs (supplemental Figures 9H-9I). Reflecting higher LSC and lower inflammatory signatures, MEIS1/ERG/MYB/FLI-1/ETV6 regulons were upregulated, while NFKB1/NFKB2/REL/RELB/AP-1 regulons were downregulated within RACs (Figure 4F). Notably, several genes upregulated within RACs are related to oncogenic MLL fusions. Accordingly, genes normally bound by menin and those that are downregulated and/or that lose menin occupancy upon menin inhibition[65-67,70] were enriched within RACs (Figure 4G). DOT1L or NPM1c targets[66,68,69] were also enriched (Figure 4G).

Finally, we asked whether relapse-associated transcriptional processes were selected by EOC3. We computed a transcriptional signature of relapse post-IVO+VEN, shared across pts 11/14/9 (Figure 4H, supplemental Figures 9J-9K, supplemental Table 5D). Several genes associated with poor prognosis in AML were upregulated within RACs, while inflammatory and AP-1 complex genes were downregulated. Strikingly, this relapse signature was already upregulated within RACs by EOC3, while patients were still in CR (Figure 4I). Similarly, other relapse-associated signatures, including menin targets, were also upregulated within RACs by EOC3 (Figure 4I, supplemental Figure 10). This suggests selection operated on these shared relapse-associated programs.

In contrast, pt4 displayed a unique transcriptional mechanism of therapy adaptation (supplemental Figure 11). Resistant clones, expanded within CMPs, showed a transcriptional erythroid bias (supplemental Figure 11B-D) and a signature of *TP53*-mutant LSCs (supplemental Figure 11E)[64] which, at least in the clone harbouring trisomy 1, may be attributed to increased *MDM4* expression (supplemental Figure 11F)[95]. Notably, AML subtypes with erythroid differentiation rely on BCL-xL for survival.[96]

Collectively, in pts 11/14/9 (AML), different somatic genetic backgrounds converge onto a transcriptional upregulation of stemness, proliferation, non-glycolytic metabolism, and menin targets. These programs are selected while patients are in CR, months prior to relapse.

Sustained treatment response is associated with eradication of leukemic clones and selection of clonal hematopoiesis with a pre-leukemic driver.

Finally, we report on 2 patients (pts 18/10) who remained in remission for 4.1 and 4.8 years, respectively, at the point of data cut-off.

Pt18 relapsed after AZA monotherapy prior to enrollment and now received IVO/VEN/AZA (supplemental Figure 12A). The BM at baseline contained *RUNX1* (R), *IDH1* (I), *SRSF2* (S), and *ASXL1* (A) mutations (Figures 5A–5B; supplemental Figures 12B–12C). The major RI/RIS clones (Figure 5B; supplemental Table 4F) were dominant within expanded LMPP/GMP compartments (Figure 5C). A minor independent *ASXL1*-mutated clone was also detected. By EOC1, when pt18 achieved CRi, the LMPP/GMP compartments shrank (Figure 5C). Mature myeloid cells represented the greatest proportion of the BM and were either WT or contained the *ASXL1*-mutant clone; the latter had expanded 4-fold at EOC1 compared to baseline (Figure 5B). At EOC9, blood production was largely sustained by *ASXL1*-mutated and WT hematopoiesis that outcompeted leukemic clones within HSPCs (Figures 5B–5C). While *ASXL1* mutations confer unfavorable prognosis in AML,[18,19,97] persistent *ASXL1* mutations at remission do not correlate with relapse in intensively treated patients.[98] We now show that clones harboring a single *ASXL1* mutation can expand with

IVO/VEN/AZA (Figures 3F and 5C) and do not necessarily associate with relapse; the prognostic impact of such clones requires further investigation.

Pt10 had been pretreated with 4 prior lines of therapy and relapsed after receiving allo-HCT. The dominant *IDH1*-R132S baseline clone also included an *IDH1*-R119P mutation, consistent with prior olutasidenib (FT-2102) treatment.[99] Remarkably, the dominant baseline clone, containing 8 driver mutations, was eradicated by EOC3 of IVO/VEN (CRi; Figures 5D–5F and supplemental Figures 13A-13B). WT donor hematopoiesis was reconstituted, with no evidence of alternative leukemic clones (Figure 5E; supplemental Tables 1J and 4G). Pt10 has remained in remission after 57 months of follow-up. In addition to eradicating leukemic/pre-leukemic clones, IVO+VEN may have given time for a donor graft versus leukemia effect. Notably, bulk NGS at remission revealed a *GNAS* mutation (1% VAF), not detected pre-treatment (supplemental Table 1H). Although not genotyped in TARGET-seq+, the mutation likely represents independent clonal hematopoiesis (CH).

Altogether, in relapsing patients, resistant clones were selected within 3 treatment cycles, in progenitor or GM precursor compartments, with concurrent reduction of the leukemic clones dominant pre-treatment (Figure 6A). By contrast, in two patients remaining in sustained remission, therapy eradicated leukemic clones from early compartments, allowing hematopoiesis from WT and CH cells.

Discussion

Prior bulk and single-cell studies from AML patients treated with either mutant IDH inhibitors,[1,26,38] FLT3 inhibitors,[100-102] or VEN+AZA[25,27] have shown that multiple genetic drivers and clones co-exist in pre-treatment samples. At relapse, diverse genetic evolution patterns occur, with selection of *RAS*, *FLT3,* and *TP53* mutations (all adverse risk prognostic mutations for VEN+AZA[103]), and karyotypic evolution (e.g. monosomy 7, complex karyotype). Furthermore, persistent leukemic mutations at remission correlate with relapse in VEN+AZA[104,105] and intensively treated patients.[98,106-108] Here, we present a first detailed study combining high fidelity single-cell genotyping (median 77% genotyping success rate, supplemental Table 3D), critical for confident assignment of clonal identity, high content scRNA-seq (median 7,602 genes/cell), and index sorting of HSPC/precursor populations in serial patient samples. This approach enabled us to identify and characterize relapse-associated clones in early post-treatment samples, within minor cell populations later expanded at relapse. Despite the limitations inherent to patient/treatment heterogeneity and cohort size, important general principles emerge.

First, therapy-driven (poly)clonal selection occurs rapidly, within 1-3 treatment cycles, both in patients who relapse and those who remain in long-term remission. Clonal selection leading

to relapse was detected in small immunophenotypic populations shown to contain LSC function in prior studies.[11,12,74] We propose that rapid clonal selection by IVO+VEN±AZA within immature BM compartments foreshadows outcome (Figure 6B).

Resistant clones were either not detected prior to treatment, or were present but presumably less fit, before gaining advantage under therapeutic pressure. Where we did not detect new genetic drivers, we cannot exclude that undetected/unknown coding or non-coding genetic drivers contributed to clonal selection. An alternative possibility is that therapy induced non-genetic chromatin reprogramming,[109] leading to transcriptional changes in the same genetic clones, as observed by others.[38] Future linkage of single-cell clonal and chromatin readouts[43,110,111] is required to test if this is influenced by epigenetic adaptation. Even where resistant clones were detected only after treatment exposure (pts 11/5/20), they may have been already present at baseline, below the detection limit of conventional approaches, as previously suggested.[38,112] Ultra-deep sequencing or ultra-sensitive targeted mutational profiling (applicable, for example, to *FLT3*-ITD) at baseline may address this issue.

Rapid clonal selection preceded treatment failure by months or years. Thus, the kinetics of initial selection did not correlate with timing of relapse. This may be due to: (a) variable clonal fitness; (b) different cell-of-origin of resistant clones; (c) clonal competition; (d) differing microenvironments; (e) variable ability of residual normal cells to sustain hematopoiesis. Though selection of pro-proliferative *FLT3*-ITD and *FLT3*-TKD mutant clones correlated with relapse, not all signaling mutations were selected, suggesting clonal context or variable signaling properties influence selective advantage.

Second, our findings emphasize the value of comparing transcriptional profiles of dominant pre-treatment and relapse clones within the same differentiation stages, relying on high efficiency single-cell genotyping. Distinct genetic backgrounds of resistant clones across patients converged onto common transcriptional processes. Resistant clones upregulated LSC/HSC self-renewal signatures, with concomitant depletion of myeloid differentiation and inflammatory signatures. Given that monocytic differentiation mediates VEN resistance, the convincing transcriptional increase in stemness observed here likely relates to IVO resistance. Moreover, non-glycolytic catabolic pathways, including BCAA catabolism, were enriched in resistant clones. The latter consumes α-KG, potentially relating to IVO resistance, while also feeding into the TCA cycle, potentially relating to VEN resistance. Perhaps the most striking finding was that menin targets were consistently upregulated in resistant clones. If validated in larger cohorts of IVO+VEN±AZA-treated patients and in relapsed AML patients more generally, these observations provide a rationale for testing menin inhibition in samples with these RNA signatures.

Crucially, these transcriptional signatures, including menin targets, were upregulated by EOC3, whilst patients were still in CR. This, coupled with the temporal window between initial clonal selection and clinical relapse, could enable MRD-directed therapies, as they become increasingly available in the context of clinical trials (e.g. the INTERCEPT Trial ANZCTR: ACTRN12621000439842). However, a key limitation of our approach is its lack of scalability to clinical practice. Our findings should provide motivation for commercial platforms[9,101,102,113,114] combined with cheaper, novel sequencing technology, to develop scalable and affordable tests.

Collectively, our study highlights a common principle that clonal selection occurs early within immature cell populations, foreshadowing outcome to IVO+VEN±AZA. It will be important to determine if our findings are validated in the recently opened, pivotal EVOLVE-1 Phase III trial, that will test IVO+VEN+AZA versus IVO+AZA+placebo. Moreover, our findings may extend to other targeted therapy combinations, as each treatment provides a selective pressure favoring the outgrowth of contextually fit clones.

Acknowledgements

P.V. acknowledges funding from the Medical Research Council (MRC) Molecular Haematology Unit Programme Grant (MC_UU_00029/8), Blood Cancer UK Programme Continuity Grant 13008, NIHR Senior Fellowship and the Oxford BRC Haematology Theme. P.V. and B.S also acknowledge previous funding from the MRC Molecular Haematology Unit Programme Grant (MC_UU_12009/11). S.T. was supported by the WIMM DPhil Prize Studentship funding from Scatcherd European Scholarship in partnership with The Medical Research Council/Radcliffe Department of Medicine and The Clarendon Fund. F.A.R. is supported by the Oxford – Sir David Weatherall Scholarship from Green Templeton College and the WIMM Prize Studentship from the MRC Weatherall Institute of Molecular Medicine. R.M. is supported by the Mildred-Scheel-Postdoc Program by the Deutsche Krebshilfe (project number 70115737). A.J.G. was supported by DPhil studentship funding from the Lady Tata Memorial Trust. C.D.D is supported by the LLS Scholar in Clinical Research Award. N.A.J. was supported by a Medical Research Council and Leukaemia UK Clinical Research Training Fellowship (MR/R002258/1). M.M., B.U., and M.A.S. were funded by the Haematology Theme of the Oxford NIHR Biomedical Research Centre. V.K. was funded by the Deutsche Forschungsgemeinschaft (DFG, German Research Foundation – project number 526169089). This research was funded in part by the NIH/NCI Cancer Center Support Grant P30 CA016672. The authors thank Prof. James Davies, Prof. Peter Valk, Prof. Michael Heuser, Dr. Susann Rahmig, Dr. David Cruz Hernandez, and Ms. Grace Meaker, for insightful comments and discussions. The authors also acknowledge the MRC

WIMM Flow Cytometry and Single Cell Facilities. Biorender was used fully or in part to generate the Visual Abstract, Figures 1B, 2E, 5E, 6B, and supplemental Figures 4C, 7F, and 12A.

Authors' Contributions

S. Turkalj: Data curation, formal analysis, investigation, methodology, visualization, software, writing-original draft, writing-review & editing. **F.A. Radtke:** Formal analysis, methodology, visualization, software, writing-original draft, writing-review & editing. **B. Stoilova:** Conceptualization, data curation, formal analysis, investigation, methodology, software, writing-review & editing. **R. Mecklenbrauck:** Data curation, visualization, writing-original draft, writing-review & editing. **A. Groom:** Investigation, methodology, writing-original draft, writing-review & editing. **N.A. Jakobsen:** Investigation, methodology, software, writing-review & editing. **C.A. Lachowiez:** Data curation, writing-review & editing. **M. Metzner:** Data curation, formal analysis, methodology, writing-review & editing. **B. Usukhbayar:** Methodology, writing-review & editing. **M.A. Salazar:** Methodology, writing-review & editing. **Z. Zeng:** writing-review & editing. **S. Loghavi:** Data curation, writing-review & editing. **J. Marvin-Peek:** Data curation, writing-review & editing. **V. Körber:** Formal analysis, visualization, writing-review & editing. **F. Ravandi:** Writing-review & editing. **G. Issa:** Writing-review & editing. **T. Kadia:** Writing-review & editing. **V. Symeonidou:** Methodology, writing-review & editing. **A.P. de Groot:** Methodology, writing-review & editing. **H. Kantarjian:** Writing-review & editing. **K. Takahashi:** Resources, writing-review & editing. **M. Konopleva:** Conceptualization, resources, writing-review & editing. **C.D. DiNardo:** Conceptualization, resources, writing-review & editing. **P. Vyas:** Conceptualization, resources, funding acquisition, supervision, project administration, writing-original draft, writing-review & editing.

Authors' Disclosures

C.A. Lachowiez: Consulting/Advisory: AbbVie, Servier, Rigel, Syndax, BMS, COTA healthcare. Research funding: AbbVie; **F. Ravandi**: Consulting/Advisory: BMS, Syros, AbbVie, Astellas, Prelude. Research funding: Astyex/Taiho, Syros, Amgen, Xencor, Prelude. **G. Issa**: Consulting/Advisory: Kura Oncology, Syndax, NuProbe, Novartis, AbbVie, Sanofi, AstraZeneca. Research funding: Celgene, Merck, Kura Oncology, Syndax, Astex, NuProbe, Novartis. **T. Kadia**: Consulting/Advisory: AbbVie, Genentech, BMS, Servier, Sellas, DrenBio. Honoraria: Novartis, Rigel. Research funding: AbbVie, Genentech, BMS, Jazz, Sellas, DrenBio, Regeneron, Amgen, Pfizer, Ascentage, Incyte, ASTEX, AstraZeneca, Cellenkos. **H. Kantarjian**: Consulting/Advisory/Honoraria: AbbVie, Amgen, Ascentage, Ipsen Biopharmaceuticals, KAHR Medical, Novartis, Pfizer, Shenzhen Target Rx, Stemline, Takeda. **M. Konopleva**: Consulting/Advisory: AbbVie, AstraZeneca, Auxenion GmbH, Bakx

Therapeutics, Boehringer, Dark Blue Therapeutics, F. Hoffmann-LaRoche, Genentech, Gilead, Immune Oncology, Janssen, Legend Biotech, MEI Pharma, Redona, Sanofi Aventis, Sellas, Menarini Group, Vincerx. Research funding: AbbVie, Allogene, AstraZeneca, Genentech, Gilead, ImmunoGen, MEI Pharma, Precision Biosciences, Rafael Pharmaceutical, Sanofi Aventis, Menarini Group. Clinical trials: AbbVie, AstraZeneca, Cellectis, Genentech, Janssen, Pfizer, Sanofi Aventis, Menarini Group. IP: Reata Pharmaceutical. **C.D. DiNardo**: Consulting/Advisory/Honoraria: AbbVie, AstraZeneca, BMS, Genentech, GenMab, GSK, Immunogen, Notable Labs, Rigel, Schrodinger, Servier, Amgen, Astellas, Gilead, Jazz, Stemline; Research Funding: AbbVie, BMS, Servier, Astex, ImmuneOnc, Cleave, Foghorn, Loxo, Rigel. **P. Vyas**: Consulting/Advisory: AbbVie, Servier, Rigel, Syndax, AstraZeneca, Debiopharm, Charm Therapeutics. Research funding: Bristol Myers Squibb. Co-founder and Board: Yellowstone Biosciences. SAB: Auron Therapeutics. No disclosures were reported by the other authors.

References

1. Quek L, David MD, Kennedy A, et al. Clonal heterogeneity of acute myeloid leukemia treated with the IDH2 inhibitor enasidenib. *Nature Medicine*. 2018;24(8):1167-1177.
2. Welch John S, Ley Timothy J, Link Daniel C, et al. The Origin and Evolution of Mutations in Acute Myeloid Leukemia. *Cell*. 2012;150(2):264-278.
3. Jan M, Snyder TM, Corces-Zimmerman MR, et al. Clonal Evolution of Preleukemic Hematopoietic Stem Cells Precedes Human Acute Myeloid Leukemia. *Science Translational Medicine*. 2012;4(149):149ra118.
4. Shlush LI, Zandi S, Mitchell A, et al. Identification of pre-leukaemic haematopoietic stem cells in acute leukaemia. *Nature*. 2014;506(7488):328-333.
5. Corces-Zimmerman MR, Hong W-J, Weissman IL, Medeiros BC, Majeti R. Preleukemic mutations in human acute myeloid leukemia affect epigenetic regulators and persist in remission. *Proceedings of the National Academy of Sciences*. 2014;111(7):2548-2553.
6. Klco Jeffery M, Spencer David H, Miller Christopher A, et al. Functional Heterogeneity of Genetically Defined Subclones in Acute Myeloid Leukemia. *Cancer Cell*. 2014;25(3):379-392.
7. Hirsch P, Zhang Y, Tang R, et al. Genetic hierarchy and temporal variegation in the clonal history of acute myeloid leukaemia. *Nature Communications*. 2016;7(1):12475.
8. van Galen P, Hovestadt V, Wadsworth Ii MH, et al. Single-Cell RNA-Seq Reveals AML Hierarchies Relevant to Disease Progression and Immunity. *Cell*. 2019;176(6):1265-1281.e1224.
9. Miles LA, Bowman RL, Merlinsky TR, et al. Single-cell mutation analysis of clonal evolution in myeloid malignancies. *Nature*. 2020;587(7834):477-482.
10. Jakobsen NA, Turkalj S, Zeng AGX, et al. Selective advantage of mutant stem cells in human clonal hematopoiesis is associated with attenuated response to inflammation and aging. *Cell Stem Cell*. 2024;31(8):1127-1144.e1117.
11. Goardon N, Marchi E, Atzberger A, et al. Coexistence of LMPP-like and GMP-like Leukemia Stem Cells in Acute Myeloid Leukemia. *Cancer Cell*. 2011;19(1):138-152.
12. Quek L, Otto GW, Garnett C, et al. Genetically distinct leukemic stem cells in human CD34− acute myeloid leukemia are arrested at a hemopoietic precursor-like stage. *Journal of Experimental Medicine*. 2016;213(8):1513-1535.
13. Bottomly D, Long N, Schultz AR, et al. Integrative analysis of drug response and clinical outcome in acute myeloid leukemia. *Cancer Cell*. 2022;40(8):850-864.e859.
14. Zeng AGX, Iacobucci I, Shah S, et al. Single-cell transcriptional mapping reveals genetic and non-genetic determinants of aberrant differentiation in AML. *bioRxiv*. 2024.
15. Hashimoto M, Saito Y, Nakagawa R, et al. Combined inhibition of XIAP and BCL2 drives maximal therapeutic efficacy in genetically diverse aggressive acute myeloid leukemia. *Nat Cancer*. 2021;2(3):340-356.

16. Zeng AGX, Bansal S, Jin L, et al. A cellular hierarchy framework for understanding heterogeneity and predicting drug response in acute myeloid leukemia. *Nature Medicine*. 2022;28(6):1212-1223.
17. Mardis ER, Ding L, Dooling DJ, et al. Recurring Mutations Found by Sequencing an Acute Myeloid Leukemia Genome. *New England Journal of Medicine*. 2009;361(11):1058-1066.
18. Papaemmanuil E, Gerstung M, Bullinger L, et al. Genomic Classification and Prognosis in Acute Myeloid Leukemia. *New England Journal of Medicine*. 2016;374(23):2209-2221.
19. Döhner H, Wei AH, Appelbaum FR, et al. Diagnosis and management of AML in adults: 2022 recommendations from an international expert panel on behalf of the ELN. *Blood*. 2022;140(12):1345-1377.
20. DiNardo CD, Jonas BA, Pullarkat V, et al. Azacitidine and Venetoclax in Previously Untreated Acute Myeloid Leukemia. *New England Journal of Medicine*. 2020;383(7):617-629.
21. Wei AH, Montesinos P, Ivanov V, et al. Venetoclax plus LDAC for newly diagnosed AML ineligible for intensive chemotherapy: a phase 3 randomized placebo-controlled trial. *Blood*. 2020;135(24):2137-2145.
22. Pratz KW, Jonas BA, Pullarkat V, et al. Long-term follow-up of VIALE-A: Venetoclax and azacitidine in chemotherapy-ineligible untreated acute myeloid leukemia. *Am J Hematol*. 2024;99(4):615-624.
23. Montesinos P, Recher C, Vives S, et al. Ivosidenib and Azacitidine in IDH1-Mutated Acute Myeloid Leukemia. *New England Journal of Medicine*. 2022;386(16):1519-1531.
24. Turkalj S, Radtke FA, Vyas P. An Overview of Targeted Therapies in Acute Myeloid Leukemia. *HemaSphere*. 2023;7(6):e914.
25. DiNardo CD, Tiong IS, Quaglieri A, et al. Molecular patterns of response and treatment failure after frontline venetoclax combinations in older patients with AML. *Blood*. 2020;135(11):791-803.
26. Choe S, Wang H, DiNardo CD, et al. Molecular mechanisms mediating relapse following ivosidenib monotherapy in IDH1-mutant relapsed or refractory AML. *Blood Advances*. 2020;4(9):1894-1905.
27. Sango J, Carcamo S, Sirenko M, et al. RAS-mutant leukaemia stem cells drive clinical resistance to venetoclax. *Nature*. 2024.
28. Moujalled DM, Brown FC, Chua CC, et al. Acquired mutations in BAX confer resistance to BH3-mimetic therapy in acute myeloid leukemia. *Blood*. 2023;141(6):634-644.
29. Waclawiczek A, Leppa AM, Renders S, et al. Combinatorial BCL2 Family Expression in Acute Myeloid Leukemia Stem Cells Predicts Clinical Response to Azacitidine/Venetoclax. *Cancer Discov*. 2023;13(6):1408-1427.
30. Kojima K, Konopleva M, Tsao T, et al. Selective FLT3 inhibitor FI-700 neutralizes Mcl-1 and enhances p53-mediated apoptosis in AML cells with activating mutations of FLT3 through Mcl-1/Noxa axis. *Leukemia*. 2010;24(1):33-43.
31. Zhang Q, Riley-Gillis B, Han L, et al. Activation of RAS/MAPK pathway confers MCL-1 mediated acquired resistance to BCL-2 inhibitor venetoclax in acute myeloid leukemia. *Signal Transduct Target Ther*. 2022;7(1):51.
32. Bhatt S, Pioso MS, Olesinski EA, et al. Reduced Mitochondrial Apoptotic Priming Drives Resistance to BH3 Mimetics in Acute Myeloid Leukemia. *Cancer Cell*. 2020;38(6):872-890 e876.
33. Pollyea DA, Stevens BM, Jones CL, et al. Venetoclax with azacitidine disrupts energy metabolism and targets leukemia stem cells in patients with acute myeloid leukemia. *Nature Medicine*. 2018;24(12):1859-1866.
34. Stevens BM, Jones CL, Pollyea DA, et al. Fatty acid metabolism underlies venetoclax resistance in acute myeloid leukemia stem cells. *Nature Cancer*. 2020;1(12):1176-1187.
35. Jones CL, Stevens BM, D'Alessandro A, et al. Inhibition of Amino Acid Metabolism Selectively Targets Human Leukemia Stem Cells. *Cancer Cell*. 2018;34(5):724-740.e724.
36. Pei S, Pollyea DA, Gustafson A, et al. Monocytic Subclones Confer Resistance to Venetoclax-Based Therapy in Patients with Acute Myeloid Leukemia. *Cancer Discov*. 2020;10(4):536-551.
37. Wang F, Morita K, DiNardo CD, et al. Leukemia stemness and co-occurring mutations drive resistance to IDH inhibitors in acute myeloid leukemia. *Nature Communications*. 2021;12(1):2607.
38. Sirenko M, Lee S, Sun Z, et al. Deconvoluting clonal and cellular architecture in IDH-mutant acute myeloid leukemia. *Cell Stem Cell*. 2025.
39. Lachowiez CA, Loghavi S, Zeng Z, et al. A Phase Ib/II Study of Ivosidenib with Venetoclax ± Azacitidine in IDH1-Mutated Myeloid Malignancies. *Blood Cancer Discovery*. 2023;4(4):276-293.

40. Rodriguez-Meira A, Buck G, Clark S-A, et al. Unravelling Intratumoral Heterogeneity through High-Sensitivity Single-Cell Mutational Analysis and Parallel RNA Sequencing. *Molecular Cell*. 2019;73(6):1292-1305.e1298.
41. Jakobsen NA, Turkalj S, Vyas P. Protocol for high-quality RNA sequencing, cell surface protein analysis, and genotyping in single cells using TARGET-seq+. *STAR Protocols*. 2025;6(2):103832.
42. Blätte TJ, Schmalbrock LK, Skambraks S, et al. getITD for FLT3-ITD-based MRD monitoring in AML. *Leukemia*. 2019;33(10):2535-2539.
43. Turkalj S, Jakobsen NA, Groom A, et al. GTAC enables parallel genotyping of multiple genomic loci with chromatin accessibility profiling in single cells. *Cell Stem Cell*. 2023;30(5):722-740.e711.
44. Hao Y, Stuart T, Kowalski MH, et al. Dictionary learning for integrative, multimodal and scalable single-cell analysis. *Nature Biotechnology*. 2024;42(2):293-304.
45. Amezquita RA, Lun ATL, Becht E, et al. Orchestrating single-cell analysis with Bioconductor. *Nature Methods*. 2020;17(2):137-145.
46. Patel AP, Tirosh I, Trombetta JJ, et al. Single-cell RNA-seq highlights intratumoral heterogeneity in primary glioblastoma. *Science*. 2014;344(6190):1396-1401.
47. Kuipers J, Jahn K, Raphael BJ, Beerenwinkel N. Single-cell sequencing data reveal widespread recurrence and loss of mutational hits in the life histories of tumors. *Genome Research*. 2017;27(11):1885-1894.
48. Finak G, McDavid A, Yajima M, et al. MAST: a flexible statistical framework for assessing transcriptional changes and characterizing heterogeneity in single-cell RNA sequencing data. *Genome Biology*. 2015;16(1):278.
49. Kumar N, Mishra B, Athar M, Mukhtar S. Inference of Gene Regulatory Network from Single-Cell Transcriptomic Data Using pySCENIC. In: Mukhtar S, ed. Modeling Transcriptional Regulation: Methods and Protocols. New York, NY: Springer US; 2021:171-182.
50. Aibar S, González-Blas CB, Moerman T, et al. SCENIC: single-cell regulatory network inference and clustering. *Nature Methods*. 2017;14(11):1083-1086.
51. Landberg N, Köhnke T, Feng Y, et al. IDH1-Mutant Preleukemic Hematopoietic Stem Cells Can Be Eliminated by Inhibition of Oxidative Phosphorylation. *Blood Cancer Discovery*. 2024;5(2):114-131.
52. Law CW, Chen Y, Shi W, Smyth GK. voom: precision weights unlock linear model analysis tools for RNA-seq read counts. *Genome Biology*. 2014;15(2):R29.
53. Hackert NS, Radtke FA, Exner T, et al. Human and mouse neutrophils share core transcriptional programs in both homeostatic and inflamed contexts. *Nature Communications*. 2023;14(1):8133.
54. Subramanian A, Tamayo P, Mootha VK, et al. Gene set enrichment analysis: A knowledge-based approach for interpreting genome-wide expression profiles. *Proceedings of the National Academy of Sciences*. 2005;102(43):15545-15550.
55. Castanza AS, Recla JM, Eby D, Thorvaldsdóttir H, Bult CJ, Mesirov JP. Extending support for mouse data in the Molecular Signatures Database (MSigDB). *Nature Methods*. 2023;20(11):1619-1620.
56. García-Prat L, Kaufmann KB, Schneiter F, et al. TFEB-mediated endolysosomal activity controls human hematopoietic stem cell fate. *Cell Stem Cell*. 2021;28(10):1838-1850.e1810.
57. Xie SZ, Kaufmann KB, Wang W, et al. Sphingosine-1-Phosphate Receptor 3 Potentiates Inflammatory Programs in Normal and Leukemia Stem Cells to Promote Differentiation. *Blood Cancer Discovery*. 2021;2(1):32-53.
58. Pietras Eric M, Reynaud D, Kang Y-A, et al. Functionally Distinct Subsets of Lineage-Biased Multipotent Progenitors Control Blood Production in Normal and Regenerative Conditions. *Cell Stem Cell*. 2015;17(1):35-46.
59. Zhang YW, Mess J, Aizarani N, et al. Hyaluronic acid–GPRC5C signalling promotes dormancy in haematopoietic stem cells. *Nature Cell Biology*. 2022;24(7):1038-1048.
60. Ng SWK, Mitchell A, Kennedy JA, et al. A 17-gene stemness score for rapid determination of risk in acute leukaemia. *Nature*. 2016;540(7633):433-437.
61. Saito Y, Kitamura H, Hijikata A, et al. Identification of Therapeutic Targets for Quiescent, Chemotherapy-Resistant Human Leukemia Stem Cells. *Science Translational Medicine*. 2010;2(17):17ra19-17ra19.
62. Voit RA, Tao L, Yu F, et al. A genetic disorder reveals a hematopoietic stem cell regulatory network co-opted in leukemia. *Nature Immunology*. 2023;24(1):69-83.

63. Xie SZ, Garcia-Prat L, Voisin V, et al. Sphingolipid Modulation Activates Proteostasis Programs to Govern Human Hematopoietic Stem Cell Self-Renewal. *Cell Stem Cell*. 2019;25(5):639-653.e637.
64. Rodriguez-Meira A, Norfo R, Wen S, et al. Single-cell multi-omics identifies chronic inflammation as a driver of TP53-mutant leukemic evolution. *Nature Genetics*. 2023;55(9):1531-1541.
65. Olsen SN, Godfrey L, Healy JP, et al. MLL::AF9 degradation induces rapid changes in transcriptional elongation and subsequent loss of an active chromatin landscape. *Molecular Cell*. 2022;82(6):1140-1155.e1111.
66. Krivtsov AV, Evans K, Gadrey JY, et al. A Menin-MLL Inhibitor Induces Specific Chromatin Changes and Eradicates Disease in Models of MLL-Rearranged Leukemia. *Cancer Cell*. 2019;36(6):660-673.e611.
67. Zhou X, Zhang L, Aryal S, et al. Epigenetic regulation of noncanonical menin targets modulates menin inhibitor response in acute myeloid leukemia. *Blood*. 2024;144(19):2018-2032.
68. Uckelmann HJ, Haarer EL, Takeda R, et al. Mutant NPM1 Directly Regulates Oncogenic Transcription in Acute Myeloid Leukemia. *Cancer Discovery*. 2023;13(3):746-765.
69. Daigle Scott R, Olhava Edward J, Therkelsen Carly A, et al. Selective Killing of Mixed Lineage Leukemia Cells by a Potent Small-Molecule DOT1L Inhibitor. *Cancer Cell*. 2011;20(1):53-65.
70. Perner F, Stein EM, Wenge DV, et al. MEN1 mutations mediate clinical resistance to menin inhibition. *Nature*. 2023;615(7954):913-919.
71. Popescu D-M, Botting RA, Stephenson E, et al. Decoding human fetal liver haematopoiesis. *Nature*. 2019;574(7778):365-371.
72. Velten L, Haas SF, Raffel S, et al. Human haematopoietic stem cell lineage commitment is a continuous process. *Nature Cell Biology*. 2017;19(4):271-281.
73. Korotkevich G, Sukhov V, Budin N, Shpak B, Artyomov MN, Sergushichev A. Fast gene set enrichment analysis. *bioRxiv*. 2021:060012.
74. Sarry J-E, Murphy K, Perry R, et al. Human acute myelogenous leukemia stem cells are rare and heterogeneous when assayed in NOD/SCID/IL2Rγc-deficient mice. *The Journal of Clinical Investigation*. 2011;121(1):384-395.
75. Pei S, Shelton IT, Gillen AE, et al. A Novel Type of Monocytic Leukemia Stem Cell Revealed by the Clinical Use of Venetoclax-Based Therapy. *Cancer Discovery*. 2023;13(9):2032-2049.
76. Lagadinou Eleni D, Sach A, Callahan K, et al. BCL-2 Inhibition Targets Oxidative Phosphorylation and Selectively Eradicates Quiescent Human Leukemia Stem Cells. *Cell Stem Cell*. 2013;12(3):329-341.
77. Dzneladze I, He R, Woolley JF, et al. INPP4B overexpression is associated with poor clinical outcome and therapy resistance in acute myeloid leukemia. *Leukemia*. 2015;29(7):1485-1495.
78. Woolley JF, Chen K, Saffi GT, et al. INPP4B drives lysosome biogenesis to restrict leukemic stem cell differentiation and promote leukemogenesis. *bioRxiv*. 2022:2021.2003.2025.437029.
79. Nguyen CH, Glüxam T, Schlerka A, et al. SOCS2 is part of a highly prognostic 4-gene signature in AML and promotes disease aggressiveness. *Scientific Reports*. 2019;9(1):9139.
80. Zuber J, Rappaport AR, Luo W, et al. An integrated approach to dissecting oncogene addiction implicates a Myb-coordinated self-renewal program as essential for leukemia maintenance. *Genes & Development*. 2011;25(15):1628-1640.
81. Wong P, Iwasaki M, Somervaille TCP, So CWE, Cleary ML. Meis1 is an essential and rate-limiting regulator of MLL leukemia stem cell potential. *Genes & Development*. 2007;21(21):2762-2774.
82. Brown FC, Still E, Koche RP, et al. MEF2C Phosphorylation Is Required for Chemotherapy Resistance in Acute Myeloid Leukemia. *Cancer Discovery*. 2018;8(4):478-497.
83. Faber J, Krivtsov AV, Stubbs MC, et al. HOXA9 is required for survival in human MLL-rearranged acute leukemias. *Blood*. 2009;113(11):2375-2385.
84. Li Z, Zhang Z, Li Y, et al. PBX3 is an important cofactor of HOXA9 in leukemogenesis. *Blood*. 2013;121(8):1422-1431.
85. Fischbach NA, Rozenfeld S, Shen W, et al. HOXB6 overexpression in murine bone marrow immortalizes a myelomonocytic precursor in vitro and causes hematopoietic stem cell expansion and acute myeloid leukemia in vivo. *Blood*. 2005;105(4):1456-1466.
86. Antonchuk J, Sauvageau G, Humphries RK. HOXB4-Induced Expansion of Adult Hematopoietic Stem Cells Ex Vivo. *Cell*. 2002;109(1):39-45.
87. Calvanese V, Nguyen AT, Bolan TJ, et al. MLLT3 governs human haematopoietic stem-cell self-renewal and engraftment. *Nature*. 2019;576(7786):281-286.
88. Knudsen KJ, Rehn M, Hasemann MS, et al. ERG promotes the maintenance of hematopoietic stem cells by restricting their differentiation. *Genes & Development*. 2015;29(18):1915-1929.

89. Tsai F-Y, Keller G, Kuo FC, et al. An early haematopoietic defect in mice lacking the transcription factor GATA-2. *Nature*. 1994;371(6494):221-226.
90. Hock H, Meade E, Medeiros S, et al. Tel/Etv6 is an essential and selective regulator of adult hematopoietic stem cell survival. *Genes & Development*. 2004;18(19):2336-2341.
91. Kharas MG, Lengner C, Al-Shahrour F, Ebert BL, Daley GQ. Msi2 Maintains Normal Hematopoietic Stem Cell Self-Renewal. *Blood*. 2011;118(21):222.
92. Raffel S, Falcone M, Kneisel N, et al. BCAT1 restricts αKG levels in AML stem cells leading to IDHmut-like DNA hypermethylation. *Nature*. 2017;551(7680):384-388.
93. Han L, Dong L, Leung K, et al. METTL16 drives leukemogenesis and leukemia stem cell self-renewal by reprogramming BCAA metabolism. *Cell Stem Cell*. 2023;30(1):52-68.e13.
94. Zhang YW, Velasco-Hernandez T, Mess J, et al. GPRC5C drives branched-chain amino acid metabolism in leukemogenesis. *Blood Advances*. 2023;7(24):7525-7538.
95. Sebert M, Gachet S, Leblanc T, et al. Clonal hematopoiesis driven by chromosome 1q/MDM4 trisomy defines a canonical route toward leukemia in Fanconi anemia. *Cell Stem Cell*. 2023;30(2):153-170.e159.
96. Kuusanmäki H, Dufva O, Vähä-Koskela M, et al. Erythroid/megakaryocytic differentiation confers BCL-XL dependency and venetoclax resistance in acute myeloid leukemia. *Blood*. 2023;141(13):1610-1625.
97. Marta P, Saman A, Mathijs AS, et al. Acquired mutations in ASXL1 in acute myeloid leukemia: prevalence and prognostic value. *Haematologica*. 2012;97(3):388-392.
98. Jongen-Lavrencic M, Grob T, Hanekamp D, et al. Molecular Minimal Residual Disease in Acute Myeloid Leukemia. *New England Journal of Medicine*. 2018;378(13):1189-1199.
99. Molenaar RJ, Wilmink JW. IDH1/2 Mutations in Cancer Stem Cells and Their Implications for Differentiation Therapy. *Journal of Histochemistry & Cytochemistry*. 2022;70(1):83-97.
100. McMahon CM, Ferng T, Canaani J, et al. Clonal Selection with RAS Pathway Activation Mediates Secondary Clinical Resistance to Selective FLT3 Inhibition in Acute Myeloid Leukemia. *Cancer Discovery*. 2019;9(8):1050-1063.
101. Morita K, Wang F, Jahn K, et al. Clonal evolution of acute myeloid leukemia revealed by high-throughput single-cell genomics. *Nature Communications*. 2020;11(1):5327.
102. Kennedy VE, Peretz CAC, Walia A, et al. RAS pathway activation drives clonal selection and monocytic differentiation in FLT3 and BCL2 inhibitor resistance. *bioRxiv*. 2025:2025.2002.2002.636108.
103. Dohner H, Pratz KW, DiNardo CD, et al. Genetic risk stratification and outcomes among treatment-naive patients with AML treated with venetoclax and azacitidine. *Blood*. 2024;144(21):2211-2222.
104. Winters AC, Minhajuddin M, Stevens BM, et al. Multi-gene measurable residual disease assessed by digital polymerase chain reaction has clinical and biological utility in acute myeloid leukemia patients receiving venetoclax/azacitidine. *Haematologica*. 2024;109(6):1766-1778.
105. Othman J, Tiong IS, O'Nions J, et al. Molecular MRD is strongly prognostic in patients with NPM1-mutated AML receiving venetoclax-based nonintensive therapy. *Blood*. 2024;143(4):336-341.
106. Short NJ, Zhou S, Fu C, et al. Association of Measurable Residual Disease With Survival Outcomes in Patients With Acute Myeloid Leukemia: A Systematic Review and Meta-analysis. *JAMA Oncology*. 2020;6(12):1890-1899.
107. Grob T, Sanders MA, Vonk CM, et al. Prognostic Value of FLT3-Internal Tandem Duplication Residual Disease in Acute Myeloid Leukemia. *Journal of Clinical Oncology*. 2023;41(4):756-765.
108. Dillon LW, Gui G, Ravindra N, et al. Measurable Residual FLT3 Internal Tandem Duplication Before Allogeneic Transplant for Acute Myeloid Leukemia. *JAMA Oncology*. 2024;10(8):1104-1110.
109. Nuno K, Azizi A, Koehnke T, et al. Convergent epigenetic evolution drives relapse in acute myeloid leukemia. *eLife*. 2024;13:e93019.
110. Turkalj S, Jakobsen NA, Groom A, Radtke FA, Vyas P. A protocol for simultaneous high-sensitivity genotyping and chromatin accessibility profiling in single cells. *STAR Protocols*. 2023;4(4):102641.
111. Izzo F, Myers RM, Ganesan S, et al. Mapping genotypes to chromatin accessibility profiles in single cells. *Nature*. 2024;629(8014):1149-1157.
112. Shlush LI, Mitchell A, Heisler L, et al. Tracing the origins of relapse in acute myeloid leukaemia to stem cells. *Nature*. 2017;547(7661):104-108.
113. Robinson TM, Bowman RL, Persaud S, et al. Single-cell genotypic and phenotypic analysis of measurable residual disease in acute myeloid leukemia. *Science Advances*. 2023;9(38):eadg0488.

114. Sciambi A, Mendoza D, Thompson K, et al. Single-Cell Multi-Omic Analysis of AML MRD Reveals Differences in Clonal Architecture between Relapse and Non-Relapse Cases. *Blood*. 2024;144(Supplement 1):1568-1568.
115. Wilson EB. Probable Inference, the Law of Succession, and Statistical Inference. *Journal of the American Statistical Association*. 1927;22(158):209-212.

Figure Legends

Figure 1. Patient cohort and experimental strategy.

(A) Swimmer plot showing response to treatment. “X” indicates time point of first best treatment response. Treatment failure (black rhombus) is defined as either disease progression or relapse. Vertical arrows indicate sampling time points. Patients are separated into two groups according to treatment response. Patients are shown in the order in which they are mentioned in the text.

(B) Left, 6 patients were treated with IVO and VEN (pts 4, 5, 9, 10, 11, and 14); 2 patients with IVO, VEN, and AZA (pts 18 and 20). 6 patients progressed (orange); 2 patients remain in remission (green). Sequential samples were studied from three time points: (a) pre-treatment (baseline, BL); (b) early treatment response (end of cycle (EOC) 1 for pts 18 and 20, EOC3 for pts 4, 5, 9, 10, 11, and 14); (c) relapse (pts 4, 9, 11, and 14), EOC9 (pt18), or EOC11 (pts 5, 10, and 20). Samples were studied by TARGET-seq+ to obtain single-cell genotype (somatic mutations obtained through targeted genotyping; copy number alterations inferred through scRNA-seq), transcriptome, and immunophenotype. Clonal, immunophenotypic, and transcriptomic information was then merged for each single cel

Figure 2. Newly detected resistant clones are selected within 3 months of treatment within immunophenotypic LSCs, months or years prior to relapse.

(A) Top, raster plot of single-cell genotyping for pt11, within all cells assigned to a clone (n = 2,471 cells). Each row represents a genotyped locus (left). The genotyped mutations are: *DNMT3A*-N757K, *NPM1*-W288fs*12, *IDH1*-R132H, *NRAS*-G12C, *FLT3*-ITD. Each column is a single cell. Colors indicate whether a cell was called wild type (WT, gray), mutant (red), undetermined (blue), or whether genotyping failed (Failed, black). Middle, clonal assignment for each cell. Color legend on the right. Due to suboptimal genotyping at the *DNMT3A* locus, the order of acquisition of the *DNMT3A* and *NPM1* mutations was uncertain. Clone abbreviations are: WT: wild type (gray). D: *DNMT3A* mutant (cyan). N: *NPM1* mutant (yellow). DN: *DNMT3A* and *NPM1* mutant (brown). DNI: *DNMT3A*, *NPM1*, and *IDH1* mutant (purple). DNINr: *DNMT3A*, *NPM1*, *IDH1*, and *NRAS* mutant (blue). DNINrF: *DNMT3A*, *NPM1*, *IDH1, NRAS*, and *FLT3* mutant (green). Bottom, most likely clonal structure for pt11 (Methods).

(B) Longitudinal changes in clone size (y-axis) within all live, Lineage-negative (Lin^-) cells (consisting of HSPC, GM precursor, and mature myeloid cells) in pt11, showing the baseline, end of cycle 3 (EOC3), and relapse time points (x-axis). Clone color-coding as in (A). The x-axis is proportional to the time (in days) relative to baseline. CR: complete remission; AML:

de novo AML. Clone size inference within live, Lin^- cells detailed in Methods (computed frequencies and confidence intervals in supplemental Table 4).

(C) Clonal composition (indicated as percentage, y-axis) of each cell population sorted by FACS (x-axis; population abbreviations as in supplemental Figure 1A) in pt11 at baseline (left), EOC3 (middle), and relapse (right). Clone color-coding as in (A). Numbers of profiled cells per population are indicated above the bars. The size of the black dots is proportional to the percentage of a given population within all live Lin^- cells at a given time point, prior to any FACS enrichment (legend on the right). The red text marks populations exceeding the mean size of the respective healthy control BM populations by more than four standard deviations.

(D) Same panel structure as in (A) but for pt5 (n = 1,583 cells). The genotyped mutations are: *TET2*-K889*, *SF3B1*-K700E, *RUNX1*-R162K, *ASXL1*-H630fs, *IDH1*-R132C. inferCNV was used for single-cell CNA calling at chromosome 5 (del(5)(q22q35) was identified by karyotyping; referred to as chr5q-). Cells black for chr5q- did not pass scRNA-seq quality control (QC; Methods). Clone abbreviations are: WT: wild type (gray). T: *TET2* mutant (dark blue). (-5q): chr5q- (cyan). (-5q)S: chr5q- and *SF3B1* mutant (green). (-5q)R: chr5q- and *RUNX1* mutant (purple). (-5q)RA: chr5q-, *RUNX1*, and *ASXL1* mutant (orange). (-5q)RAI: chr5q-, *RUNX1*, *ASXL1,* and *IDH1* mutant (blue).

(E) Same panel structure as in (B) but for pt5, showing the baseline, EOC3, and EOC11 time points. Clone color-coding as in (D). Right, 40 months following EOC11, pt5 developed MDS associated with del(5)(q22q35) and *SF3B1*-K700E.

(F) Same panel structure as in (C) but for pt5, across baseline, EOC3, and EOC11 time points. Clone color-coding as in (D). In this patient, Lineage-positive (Lin^+) cells were also genotyped.

Figure 3. Minor pre-existing resistant clones expand within the first 3 treatment cycles within immunophenotypic LSCs.

(A) Same panel structure as in Figure 2A, but for pt14 (n = 1,296 cells). The genotyped mutations are: *DNMT3A*-G543C, *NPM1*-W288fs*12, *IDH1*-R132H. inferCNV was used for single-cell copy number alteration (CNA) calling at chromosomes 4, 21, and 20 (+4, +20, and +21 were identified by karyotyping - referred to as chr4+, chr20+, and chr21+, respectively). Clone abbreviations are: WT: wild type (gray). D: *DNMT3A* mutant (yellow). DN: *DNMT3A* and *NPM1* mutant (red). DNI: *DNMT3A*, *NPM1*, and *IDH1* mutant (blue). DN(+4): *DNMT3A*, and *NPM1* mutant with chr4+ (brown). DN(+4+21): *DNMT3A* and *NPM1* mutant with chr4+ and chr21+ (green). DN(+4+20): *DNMT3A* and *NPM1* mutant with chr4+ and chr20+ (purple).

(B) Same panel structure as in Figure 2B but for pt14. Clone color-coding as in (A).

(C) Same panel structure as in Figure 2C but for pt14.

(D) Same panel structure as in (A) but for pt9 (n = 2,885 cells). The genotyped mutations are: *ASXL1*-Q512*, *NRAS*-G13R, *IDH1*-R132C, *STAG2*-R1033*, *FLT3*-D835H. Additionally, inferCNV was used for single-cell copy number alteration (CNA) calling at chromosomes 5 and 11 (del(5)(q22q33) and +11 were identified by karyotyping; referred to as chr5q- and chr11+, respectively). Cells black for chr5q- and chr11+ did not pass scRNA-seq QC (Methods). Clone abbreviations are: WT: wild type (gray). A: *ASXL1* mutant (orange). AN: *ASXL1* and *NRAS* mutant (cyan). AI: *ASXL1* and *IDH1* mutant (blue). AIS: *ASXL1*, *IDH1*, and *STAG2* mutant (purple). AISF: *ASXL1*, *IDH1*, *STAG2,* and *FLT3* mutant (green). AI(-5q): *ASXL1* and *IDH1* mutant with chr5q- (yellow). AI(-5q+11): *ASXL1* and *IDH1* mutant with chr5q- and chr11+ (brown).

(E) Same panel structure as in (B) but for pt9. Clone color-coding as in (D). R/R AML: relapsed/refractory AML.

(F) Same panel structure as in (C) but for pt9. Clone color-coding as in (D).

Figure 4. By EOC3, resistant genetic clones transcriptionally upregulate stemness, non-glycolytic catabolism, and menin targets, while attenuating inflammation.

(A) Dominant clones at baseline (blue) and at relapse (red) were compared within the immunophenotypic LSC populations (GM precursors in pts 11/14; LMPP/GMP in pt9; CMP in pt4). Cell numbers (format: clone-population-patient-timepoint): DNI-Precursor-pt11-baseline(BL): 141; DNINr-Precursor-pt11-BL: 163; DNINrF-Precursor-pt11-relapse(REL): 392; DNI-Precursor-pt14-BL: 72; DN(+4)-Precursor-pt14-REL: 252; AI(-5q+11)-LMPP-pt9-BL: 64; AI(-5q+11)-GMP-pt9-BL: 177; AISF-LMPP-pt9-REL: 150; AISF-GMP-pt9-REL: 331; SIAJ-CMP-pt4-BL: 623; SIA(-20q+1)-CMP-pt4-REL: 141; SIA(-20q-7)-CMP-pt4-REL: 120.

(B) Above, GSEA against the genes downregulated by experimental introduction of *IDH1*-R132H mutations into human HSPCs (*IDH1*-R132H DOWN signature), comparing dominant resistant and baseline clones within expanded immunophenotypic LSC populations in pts 11/14/9. The clones compared and cell numbers are detailed in the legend for Figure 4A. The color coding corresponds to the normalized enrichment score (NES). Signatures colored in red and blue are enriched and depleted in relapse versus baseline clones, respectively; those colored in grey are non-significant (FDR > 0.05). The dot size is proportional to the -$\log_{10}$(FDR) (legend on the right). Below, rank plot of GSEA results where the *IDH*-R132H DOWN signature is labelled in red (rank reported above). The rank (y-axis) is given by multiplying -$\log_{10}(p_{adj})$ by the $\log_2$FC sign.

(C) GSEA as in B but against selected gene signatures of non-glycolytic metabolic pathways associated with venetoclax resistance.

(D) GSEA as in B but against selected HSC, LSC, branched-chain amino acid (BCAA) metabolism, and differentiation gene signatures.

(E) Heatmap of 59 genes functionally linked to HSC/LSC self-renewal (supplemental Methods). Each column represents a different comparison (supplemental Figure 9A). Colors indicate $\log_2$FC between resistant and baseline clones, symbols indicate significance. Rows are split by genes on average upregulated (mean $\log_2$FC > 0) versus downregulated (mean $\log_2$FC < 0). Within those groups, genes have been sorted by number of significant results, and ties resolved by sorting by average $\log_2$FC across the comparisons. $\log_2$FC values capped at 5. None of the samples met expression thresholds for the *HOXC4* gene. Hence, even if present in the signature, *HOXC4* is not shown in the heatmap.

(F) As in E but plotting the differential regulon activity as derived by pySCENIC (supplemental Methods). For each comparison, the corresponding regulon activity matrices were extracted. The color and symbols indicate the result of a Wilcoxon rank sum test.

(G) GSEA as in B but against selected signatures of genes sensitive to menin inhibition, DOT1L inhibition, or mutant NPM1 (NPM1c) target genes.

(H) Left, comparisons were performed as detailed in Figure 4A and supplemental Figure 9A, for pts 11/14/9. A list of genes up- or down-regulated at relapse shared across these patients was computed with a Fisher's combined probability test (supplemental Methods). Right, volcano plot of joint analysis for pts 11/14/9. The x-axis depicts the average $\log_2$FC across the respective comparisons (dominant clones at relapse versus baseline) across pts 11/14/9, the y-axis depicts the $-\log_{10}$ of the adjusted p value (Fisher's combined test). The dashed horizontal line marks the significance cutoff based on the elbow plot (supplemental Methods and supplemental Figure 9J). Dashed vertical lines indicate the ± 0.5 $\log_2$FC thresholds. Genes fulfilling those thresholds are colored based on their respective average $\log_2$FC. The dot size indicates $-\log_{10}$(adjusted p value) × $|\log_2 FC|$. Selected AP-1 genes, inflammatory genes, or genes associated with poor prognosis in AML are labelled.

(I) Violin plots of single-cell gene set representation (AUCell score) for selected gene sets, comparing the dominant baseline clone with the dominant resistant clone at the EOC3 and relapse, within the relevant cell populations. Each dot is a single cell. For each gene set, pairwise comparisons were performed between the baseline and other groups using two-sample t-tests, and the resulting p values were Benjamini-Hochberg-adjusted. The clones and number of cells analyzed at baseline/relapse are stated in the legend for Figure 4A. Cell

numbers analyzed at EOC3 are: DNINrF-Precursor-pt11: 230; DN(+4)-Precursor-pt14: 68; AISF-GMP-pt9: 8. * p <= 0.05; ** p <= 0.01; *** p <= 0.001; **** p <= 0.0001.

Figure 5. Eradication of leukemic clones, selection of independent clonal hematopoiesis, and reconstitution of WT differentiation correlates with sustained response.

(A) Same panel structure as in Figure 2A but for pt18 (n = 1,223 cells). The genotyped mutations are: *ASXL1*-W583*, *RUNX1*-R204Q, *IDH1*-R132H, *SRSF2*-P95_R102del. Clone abbreviations are: WT: wild type (gray). A: *ASXL1* mutant (dark blue). R: *RUNX1* mutant (purple). RI: *RUNX1* and *IDH1* mutant (orange). RIS: *RUNX1*, *IDH1*, and *SRSF2* mutant (blue).

(B) Same panel structure as in Figure 2B but for pt18, showing the baseline, EOC1, and EOC9 time points. Clone color-coding as in (A). sAML: secondary AML; CRi: complete remission with incomplete hematologic recovery.

(C) Same panel structure as in Figure 2C but for pt18, across baseline, EOC1, and EOC9 time points. Clone color-coding as in (A).

(D) Same panel structure as in Figure 2A but for pt10 (n = 1,446 cells). The genotyped mutations are: *BRINP3*-R68W, *SRSF2*-P95H, *NPM1*-W288fs*12, *DNMT3A*-R771Q, *KRAS*-C180X, *IDH1*-R132S, *RAD21*-E526fs*9, *IDH1*-R119P, *PTPN11*-G503E, and *WT1*-R462Q. Clone abbreviations are: WT: wild-type (gray). BSNDKIW: *BRINP3*, *SRSF2*, *NPM1*, *DNMT3A*, *KRAS*, *IDH1* (R132S), and *WT1* mutant (orange). BSNDKIRI: *BRINP3*, *SRSF2*, *NPM1*, *DNMT3A*, *KRAS*, *IDH1* (R132S), *RAD21*, and *IDH1* (R119P) mutant (blue). BSNDKIRIP: *BRINP3*, *SRSF2*, *NPM1*, *DNMT3A*, *KRAS*, *IDH1* (R132S), *RAD21*, *IDH1* (R119P), and *PTPN11* mutant (green). The order of mutation acquisition prior to the BSNDKIRI clone was unclear.

(E) Above, pt10 was pre-treated with 5 lines of therapy: (a) azacitidine (AZA); (b) idarubicin, cytarabine (IA), and the CXCR4 peptide antagonist LY2510924; (c) decitabine; (d) olutasidenib (OLU) with AZA; (e) allo-HCT. Following relapse post-allo-HCT, the patient was enrolled in the trial. Below, as in Figure 2B but for pt10, showing the baseline, EOC3, and EOC11 time points. Clone color-coding as in (D). A *GNAS*-R201H mutation, not detected at baseline, was detected at remission at 1% VAF via the bulk targeted NGS panel but was not genotyped by TS+. Chimerism results at remission are shown within the plot. Inferred clone sizes in supplemental Table 4.

(F) As in Figure 2C but for pt10, at baseline (left), EOC3 (middle), and EOC11 (right) time points. Clone color-coding as in (C).

Figure 6. Rapid clonal selection within immature cell populations foreshadows patient outcome.

(A) Line graphs showing longitudinal changes in clonal composition (indicated as % of all cells in a specific immunophenotypically-defined population, y-axis) in all studied patients (columns). The immunophenotypically-defined populations are indicated above. Clone abbreviations are indicated within the graphs. Clones associated with resistance are indicated in green; dominant pre-treatment clones sensitive to treatment are indicated in purple; the cumulative frequency of WT cells and clones harboring a single pre-leukemic driver mutation (i.e. CH clones) are indicated in grey. Dominant clones are defined as those clones contributing to at least 50% of the expanded immunophenotypic population, after arrangement in decreasing frequency (for multiple clones, the sum of their frequency was considered). Error bars depict the 95% confidence intervals calculated using the Wilson score interval.[115] Time points are indicated on the x-axis.

(B) Proposed model depicting the establishment of the clonal foundations of either treatment failure (left) or sustained response (right), early during treatment.

1002 **Table 1. Patient characteristics.**

Characteristic	Pt11	Pt5	Pt20	Pt14	Pt9	Pt4	Pt18	Pt10
Age at time of enrollment (years)	65	84	63	80	77	68	75	72
Sex	Female	Female	Male	Female	Male	Male	Male	Female
Diagnosis	AML	AML	AML	AML*	R/R AML	MDS/MPN	sAML	R/R AML
ECOG PS	1	1	1	2	2	1	0	1
Previous therapies for myeloid malignancy	NA	NA	NA	NA	DEC	AZA; FT2102	AZA	AZA; IA/LY251092; DEC; AZA/FT-2102; alloHCT
Previous $IDH1^{MUT}$ inhibitor	No	No	No	No	No	Yes	No	Yes
WBC at baseline (10^3/ml)	11	1.5	1.2	3.7	0.6	4.6	1.8	1.9
Hb at baseline (g/dl)	10.1	9.4	10.1	8	8.9	11.2	8.7	7.7
Platelets at baseline (10^3/ml)	53	185	6	57	5	160	74	12
Blast count at baseline (%)	28	47	79	16	61	12	10	23
IDH1-R132 mutation at baseline (VAF [%])	R132H (29)	R132H (22)	R132C (42)	R132H (32)	R132C (31)	R132H (38)	R132H (17)	R132S (18)
Treatment	IVO 500mg + VEN 800mg	IVO 500mg + VEN 400mg	IVO 500mg + VEN 400mg + AZA 75mg/m^2	IVO 500mg + VEN 800mg	IVO 500mg + VEN 800mg	IVO 500mg + VEN 400mg	IVO 500mg + VEN 400mg + AZA 75mg/m^2	IVO 500mg + VEN 800mg
Time on treatment (months)	3.9	49.6	26.8	9.5	6.5	13.7	49.0	57.8
Treatment failure	Yes	Yes	Yes	Yes	Yes	Yes	No	No
Duration of response (months)	3.4	47.5	24.3	6.7	3.9	12.7	48.1	57.0
Best response	CR	CR	MLFS	CR	CR	CR	CRi	CR
Overall survival (months)	5.1	62.0	31.3	52.6	7.8	42	49.0	57.8
Survival status	Deceased	Alive	Deceased	Alive	Deceased	Deceased	Alive	Alive
Somatic alterations contained within the dominant clone(s) at baseline	*DNMT3A, NPM1, IDH1, NRAS*	del(5)(q22q35), *RUNX1, ASXL1, IDH1*	*TET2, TET2, ASXL1, SRFS2, IDH1*	*DNMT3A, NPM1, IDH1*	(a) *ASXL1, IDH1, STAG2*; (b) *ASXL1, IDH1,* del(5)(q22q33), trisomy 11	*SRSF2, IDH1, ASXL2, JAK2, CBL*	*RUNX1, IDH1, SRSF2*	*BRINP3, SRSF2, NPM1, DNMT3A, KRAS, IDH1*-R132, *RAD21, IDH1*-R119
Somatic alterations contained within the dominant clone at relapse	*DNMT3A, NPM1, IDH1, NRAS, FLT3*-ITD	del(5)(q22q35), *SF3B1*	*TET2, TET2, ASXL1, SRFS2, RUNX1*	*DNMT3A, NPM1,* trisomy 4	*ASXL1, IDH1, STAG2, FLT3*-TKD	Multiple clones containing *SRSF2, IDH1, ASXL2,* and CNAs	NA	NA
Follow-up treatment	FIA/gilteritinib	LEN	VEN/HHT	Alternating CLAD/LDAC and DEC/VEN	Gilteritinib/VEN	CLAD/LDAC	NA	NA

AML: De novo acute myeloid leukemia; sAML: Secondary acute myeloid leukemia; MDS/MPN: Myelodysplastic/myeloproliferative neoplasm; R/R AML: Relapsed/refractory acute myeloid leukemia; ECOG: Eastern Cooperative Oncology Group Performance Status Scale; Hb: Hemoglobin; WBC: White blood cell count; VAF: Variant allele frequency; IVO: Ivosidenib; VEN: Venetoclax; AZA: Azacitidine; CR: Complete remission; CRi: CR with incomplete hematologic recovery; MLFS: Morphologic leukemia-free stateDEC, decitabine; AZA, azacitidine; IA, idarubicin/cyatarabine; alloHCT, allogeneic hematopoietic stem cell transplantation; LEN, lenalidomide; CLAD, cladribine; LDAC, low-dose cytarabine.

* pt14 has originally been classified as MDS/MPN (Lachowiez et al.,2023). According to ICC 2022, for this study, pt14 was re-classified as AML with mutated NPM1 (due to the presence of high NPM1 VAF and blasts > 10% at baseline).

Figure 1

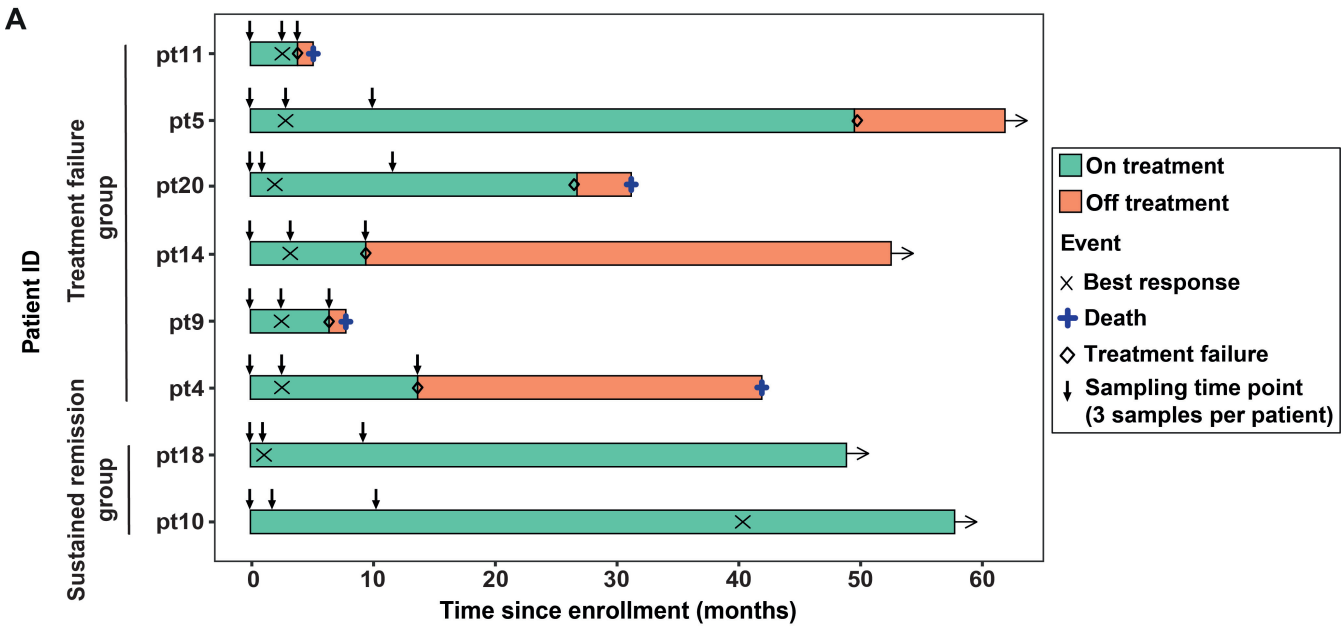
A
Patient ID
Treatment failure group
Sustained remission group
pt11
pt5
pt20
pt14
pt9
pt4
pt18
pt10
0
10
20
30
40
50
60
Time since enrollment (months)
On treatment
Off treatment
Event
Best response
Death
Treatment failure
Sampling time point
(3 samples per patient)

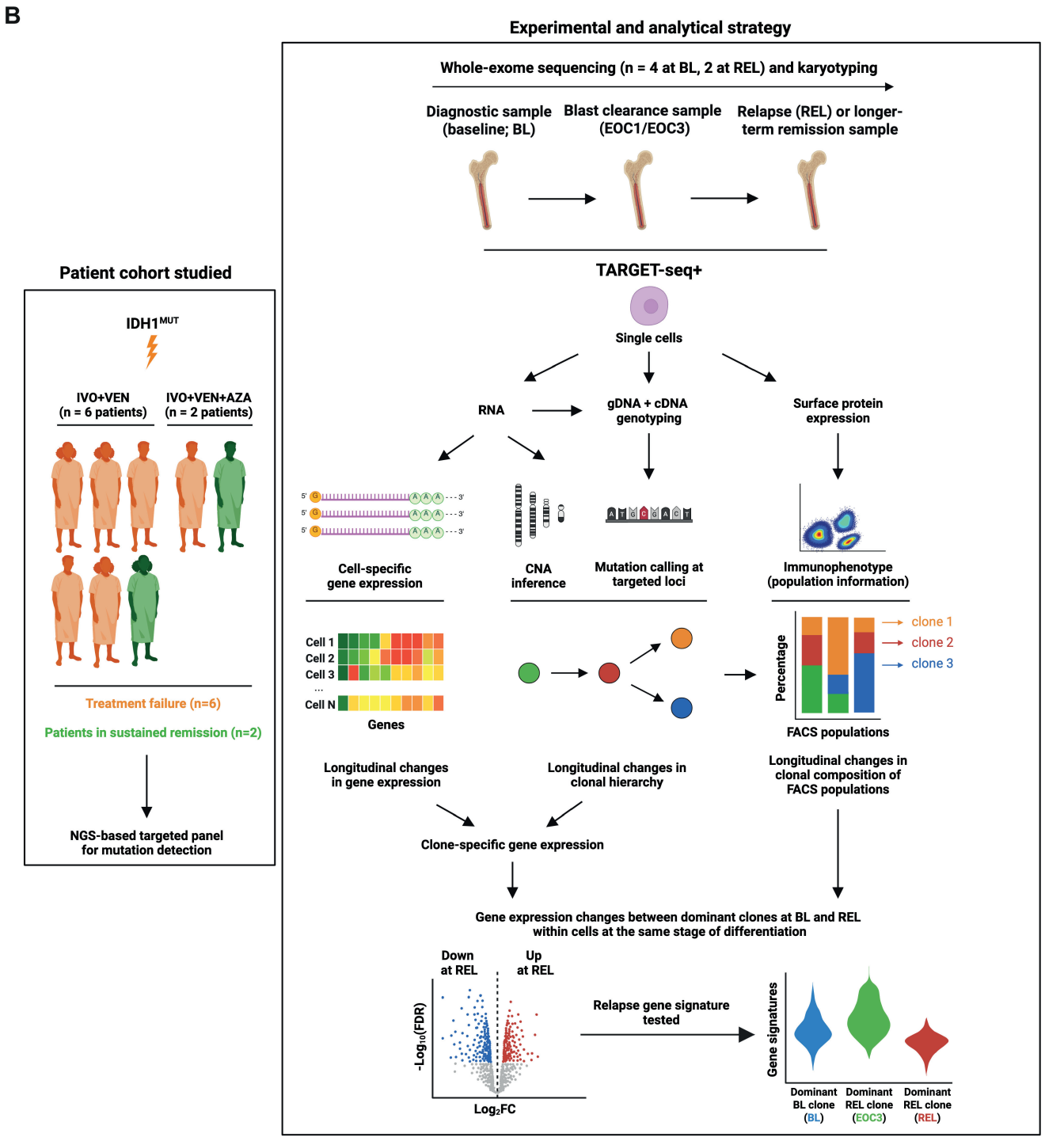
B
Experimental and analytical strategy
Whole-exome sequencing (n = 4 at BL, 2 at REL) and karyotyping
Diagnostic sample (baseline; BL)
Blast clearance sample (EOC1/EOC3)
Relapse (REL) or longer-term remission sample
Patient cohort studied
IDH1MUT
IVO+VEN (n = 6 patients)
IVO+VEN+AZA (n = 2 patients)
Treatment failure (n=6)
Patients in sustained remission (n=2)
NGS-based targeted panel for mutation detection
TARGET-seq+
Single cells
RNA
gDNA + cDNA genotyping
Surface protein expression
Cell-specific gene expression
CNA inference
Mutation calling at targeted loci
Immunophenotype (population information)
Cell 1
Cell 2
Cell 3
Cell N
Genes
clone 1
clone 2
clone 3
Percentage
FACS populations
Longitudinal changes in gene expression
Longitudinal changes in clonal hierarchy
Longitudinal changes in clonal composition of FACS populations
Clone-specific gene expression
Gene expression changes between dominant clones at BL and REL within cells at the same stage of differentiation
Down at REL
Up at REL
-Log10(FDR)
Log2FC
Relapse gene signature tested
Gene signatures
Dominant BL clone (BL)
Dominant REL clone (EOC3)
Dominant REL clone (REL)

Figure 2

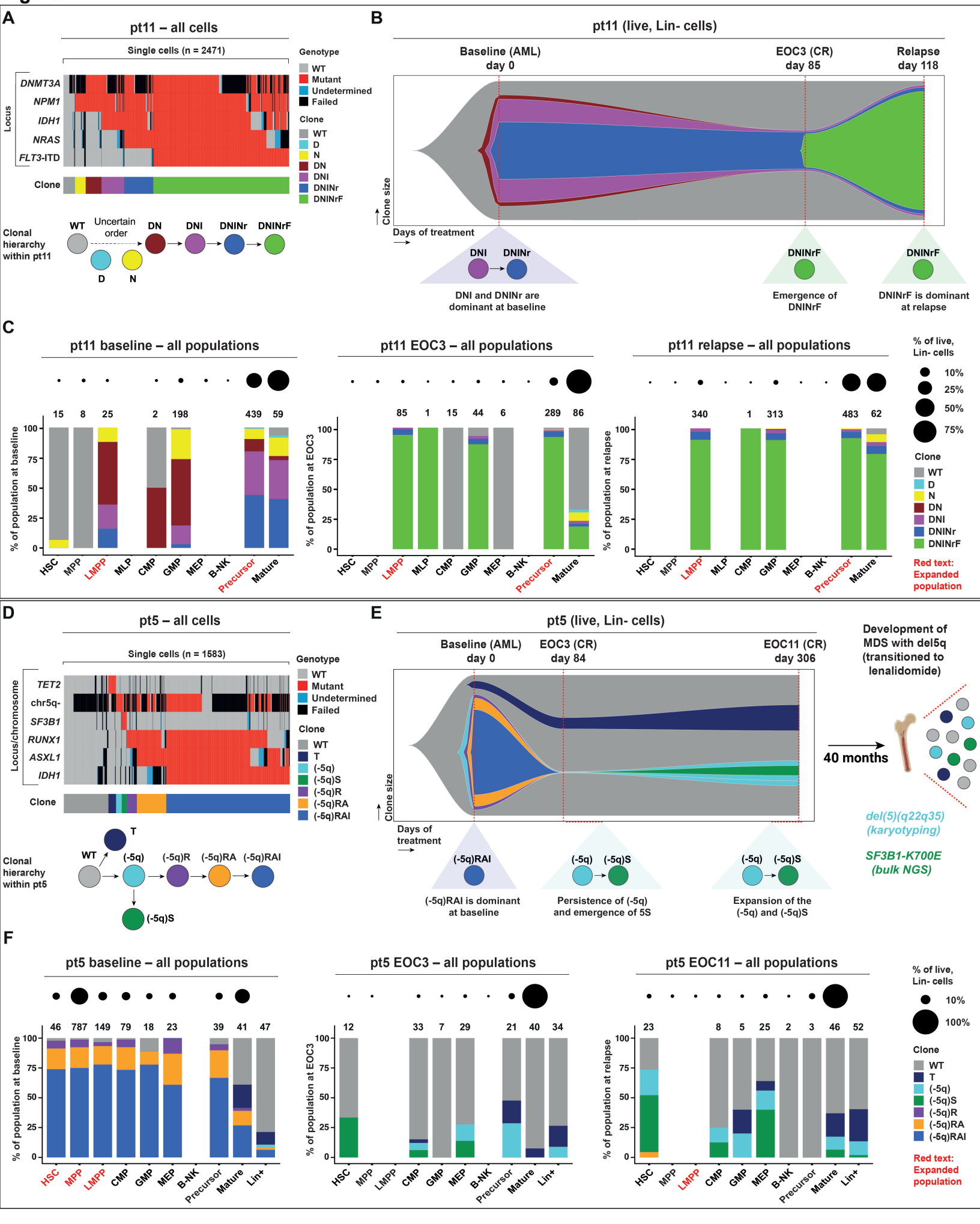
A
pt11 – all cells
Single cells (n = 2471)
DNMT3A
NPM1
IDH1
NRAS
FLT3-ITD
Locus
Clone
Genotype
WT
Mutant
Undetermined
Failed
Clone
WT
D
N
DN
DNI
DNINr
DNINrF
Clonal hierarchy within pt11
WT
Uncertain order
DN
DNI
DNINr
DNINrF
D
N
B
pt11 (live, Lin- cells)
Baseline (AML) day 0
EOC3 (CR) day 85
Relapse day 118
Clone size
Days of treatment
DNI
DNINr
DNI and DNINr are dominant at baseline
DNINrF
Emergence of DNINrF
DNINrF
DNINrF is dominant at relapse
C
pt11 baseline – all populations
pt11 EOC3 – all populations
pt11 relapse – all populations
% of population at baseline
% of population at EOC3
% of population at relapse
15 8 25 2 198 439 59
85 1 15 44 6 289 86
340 1 313 483 62
HSC MPP LMPP MLP CMP GMP MEP B-NK Precursor Mature
% of live, Lin- cells
10%
25%
50%
75%
Clone
WT
D
N
DN
DNI
DNINr
DNINrF
Red text: Expanded population
D
pt5 – all cells
Single cells (n = 1583)
TET2
chr5q-
SF3B1
RUNX1
ASXL1
IDH1
Locus/chromosome
Clone
Genotype
WT
Mutant
Undetermined
Failed
Clone
WT
T
(-5q)
(-5q)S
(-5q)R
(-5q)RA
(-5q)RAI
Clonal hierarchy within pt5
WT
T
(-5q)
(-5q)R
(-5q)RA
(-5q)RAI
(-5q)S
E
pt5 (live, Lin- cells)
Baseline (AML) day 0
EOC3 (CR) day 84
EOC11 (CR) day 306
Clone size
Days of treatment
(-5q)RAI
(-5q)RAI is dominant at baseline
(-5q)
(-5q)S
Persistence of (-5q) and emergence of 5S
(-5q)
(-5q)S
Expansion of the (-5q) and (-5q)S
Development of MDS with del5q (transitioned to lenalidomide)
40 months
del(5)(q22q35) (karyotyping)
SF3B1-K700E (bulk NGS)
F
pt5 baseline – all populations
pt5 EOC3 – all populations
pt5 EOC11 – all populations
% of population at baseline
% of population at EOC3
% of population at relapse
46 787 149 79 18 23 39 41 47
12 33 7 29 21 40 34
23 8 5 25 2 3 46 52
HSC MPP LMPP CMP GMP MEP B-NK Precursor Mature Lin+
% of live, Lin- cells
10%
100%
Clone
WT
T
(-5q)
(-5q)S
(-5q)R
(-5q)RA
(-5q)RAI
Red text: Expanded population

Figure 3

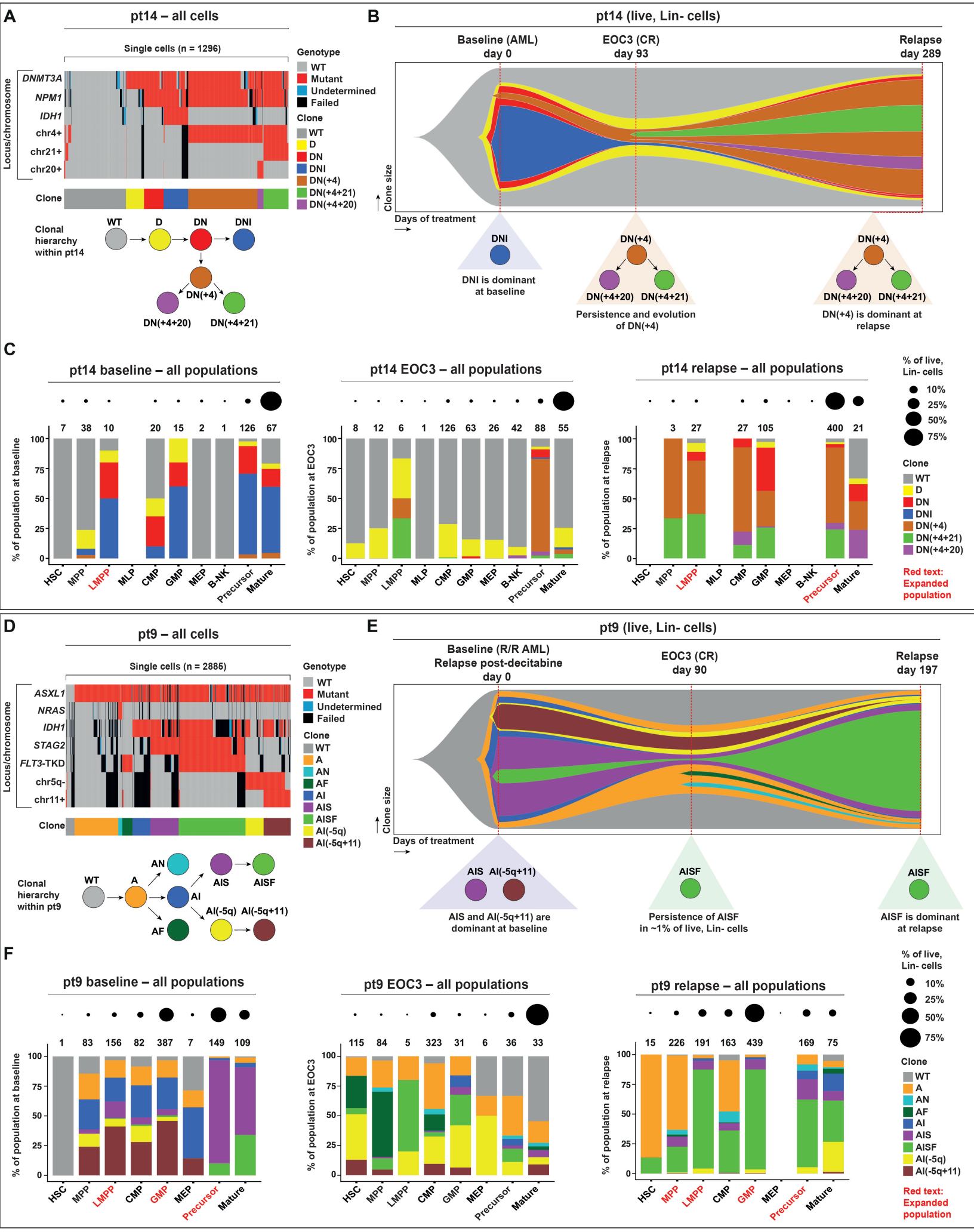
A
pt14 – all cells
Single cells (n = 1296)
Locus/chromosome
DNMT3A
NPM1
IDH1
chr4+
chr21+
chr20+
Clone
Genotype
WT
Mutant
Undetermined
Failed
Clone
WT
D
DN
DNI
DN(+4)
DN(+4+21)
DN(+4+20)
Clonal hierarchy within pt14
WT
D
DN
DNI
DN(+4)
DN(+4+20)
DN(+4+21)
B
pt14 (live, Lin- cells)
Baseline (AML) day 0
EOC3 (CR) day 93
Relapse day 289
Clone size
Days of treatment
DNI
DNI is dominant at baseline
DN(+4)
DN(+4+20)
DN(+4+21)
Persistence and evolution of DN(+4)
DN(+4)
DN(+4+20)
DN(+4+21)
DN(+4) is dominant at relapse
C
pt14 baseline – all populations
pt14 EOC3 – all populations
pt14 relapse – all populations
% of population at baseline
% of population at EOC3
% of population at relapse
7 38 10 20 15 2 1 126 67
8 12 6 1 126 63 26 42 88 55
3 27 27 105 400 21
HSC MPP LMPP MLP CMP GMP MEP B-NK Precursor Mature
% of live, Lin- cells
10%
25%
50%
75%
Clone
WT
D
DN
DNI
DN(+4)
DN(+4+21)
DN(+4+20)
Red text: Expanded population
D
pt9 – all cells
Single cells (n = 2885)
Locus/chromosome
ASXL1
NRAS
IDH1
STAG2
FLT3-TKD
chr5q-
chr11+
Clone
Genotype
WT
Mutant
Undetermined
Failed
Clone
WT
A
AN
AF
AI
AIS
AISF
AI(-5q)
AI(-5q+11)
Clonal hierarchy within pt9
WT
A
AN
AF
AI
AIS
AISF
AI(-5q)
AI(-5q+11)
E
pt9 (live, Lin- cells)
Baseline (R/R AML) Relapse post-decitabine day 0
EOC3 (CR) day 90
Relapse day 197
Clone size
Days of treatment
AIS AI(-5q+11)
AIS and AI(-5q+11) are dominant at baseline
AISF
Persistence of AISF in ~1% of live, Lin- cells
AISF
AISF is dominant at relapse
F
pt9 baseline – all populations
pt9 EOC3 – all populations
pt9 relapse – all populations
% of population at baseline
% of population at EOC3
% of population at relapse
1 83 156 82 387 7 149 109
115 84 5 323 31 6 36 33
15 226 191 163 439 169 75
HSC MPP LMPP CMP GMP MEP Precursor Mature
% of live, Lin- cells
10%
25%
50%
75%
Clone
WT
A
AN
AF
AI
AIS
AISF
AI(-5q)
AI(-5q+11)
Red text: Expanded population

Figure 4

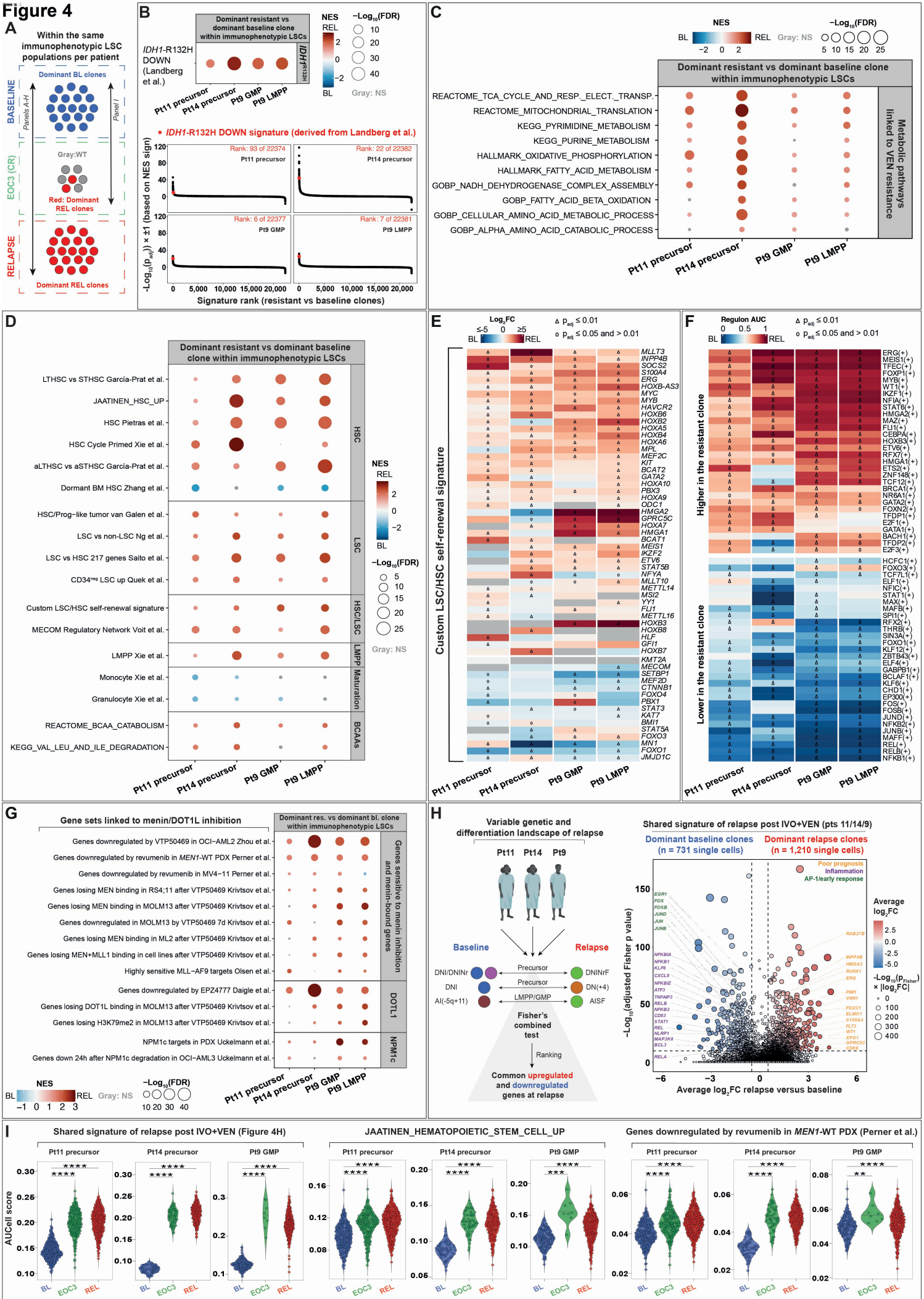
A
Within the same immunophenotypic LSC populations per patient
Dominant BL clones
BASELINE
Panels A-H
Panel I
Gray:WT
EOC3 (CR)
Red: Dominant REL clones
RELAPSE
Dominant REL clones
B
Dominant resistant vs dominant baseline clone within immunophenotypic LSCs
IDH1-R132H DOWN (Landberg et al.)
IDH1-R132H
NES
REL
BL
Gray: NS
−Log10(FDR)
Pt11 precursor
Pt14 precursor
Pt9 GMP
Pt9 LMPP
• IDH1-R132H DOWN signature (derived from Landberg et al.)
Rank: 93 of 22374
Rank: 22 of 22382
Rank: 6 of 22377
Rank: 7 of 22381
-Log10(padj) × ±1 (based on NES sign)
Signature rank (resistant vs baseline clones)
C
Dominant resistant vs dominant baseline clone within immunophenotypic LSCs
REACTOME_TCA_CYCLE_AND_RESP._ELECT._TRANSP.
REACTOME_MITOCHONDRIAL_TRANSLATION
KEGG_PYRIMIDINE_METABOLISM
KEGG_PURINE_METABOLISM
HALLMARK_OXIDATIVE_PHOSPHORYLATION
HALLMARK_FATTY_ACID_METABOLISM
GOBP_NADH_DEHYDROGENASE_COMPLEX_ASSEMBLY
GOBP_FATTY_ACID_BETA_OXIDATION
GOBP_CELLULAR_AMINO_ACID_METABOLIC_PROCESS
GOBP_ALPHA_AMINO_ACID_CATABOLIC_PROCESS
Metabolic pathways linked to VEN resistance
D
Dominant resistant vs dominant baseline clone within immunophenotypic LSCs
LTHSC vs STHSC Garcia-Prat et al.
JAATINEN_HSC_UP
HSC Pietras et al.
HSC Cycle Primed Xie et al.
aLTHSC vs aSTHSC Garcia-Prat et al.
Dormant BM HSC Zhang et al.
HSC/Prog-like tumor van Galen et al.
LSC vs non-LSC Ng et al.
LSC vs HSC 217 genes Saito et al.
CD34neg LSC up Quek et al.
Custom LSC/HSC self-renewal signature
MECOM Regulatory Network Voit et al.
LMPP Xie et al.
Monocyte Xie et al.
Granulocyte Xie et al.
REACTOME_BCAA_CATABOLISM
KEGG_VAL_LEU_AND_ILE_DEGRADATION
HSC
LSC
HSC/LSC
LMPP Maturation
BCAAs
E
Log2FC
Custom LSC/HSC self-renewal signature
F
Regulon AUC
Higher in the resistant clone
Lower in the resistant clone
G
Gene sets linked to menin/DOT1L inhibition
Genes downregulated by VTP50469 in OCI−AML2 Zhou et al.
Genes downregulated by revumenib in MEN1-WT PDX Perner et al.
Genes downregulated by revumenib in MV4−11 Perner et al.
Genes losing MEN binding in RS4;11 after VTP50469 Krivtsov et al.
Genes losing MEN binding in MOLM13 after VTP50469 Krivtsov et al.
Genes downregulated in MOLM13 by VTP50469 7d Krivtsov et al.
Genes losing MEN binding in ML2 after VTP50469 Krivtsov et al.
Genes losing MEN+MLL1 binding in cell lines after VTP50469 Krivtsov et al.
Highly sensitive MLL−AF9 targets Olsen et al.
Genes downregulated by EPZ4777 Daigle et al.
Genes losing DOT1L binding in MOLM13 after VTP50469 Krivtsov et al.
Genes losing H3K79me2 in MOLM13 after VTP50469 Krivtsov et al.
NPM1c targets in PDX Uckelmann et al.
Genes down 24h after NPM1c degradation in OCI−AML3 Uckelmann et al.
Genes sensitive to menin inhibition and menin-bound genes
DOT1L
NPM1c
H
Variable genetic and differentiation landscape of relapse
Pt11
Pt14
Pt9
Baseline
Relapse
DNI/DNINr
DNINrF
DNI
DN(+4)
AI(-5q+11)
AISF
Precursor
LMPP/GMP
Fisher's combined test
Ranking
Common upregulated and downregulated genes at relapse
Shared signature of relapse post IVO+VEN (pts 11/14/9)
Dominant baseline clones (n = 731 single cells)
Dominant relapse clones (n = 1,210 single cells)
Poor prognosis
Inflammation
AP-1/early response
-Log10(adjusted Fisher p value)
Average log2FC relapse versus baseline
Average log2FC
I
Shared signature of relapse post IVO+VEN (Figure 4H)
JAATINEN_HEMATOPOIETIC_STEM_CELL_UP
Genes downregulated by revumenib in MEN1-WT PDX (Perner et al.)
AUCell score
BL
EOC3
REL

Figure 5

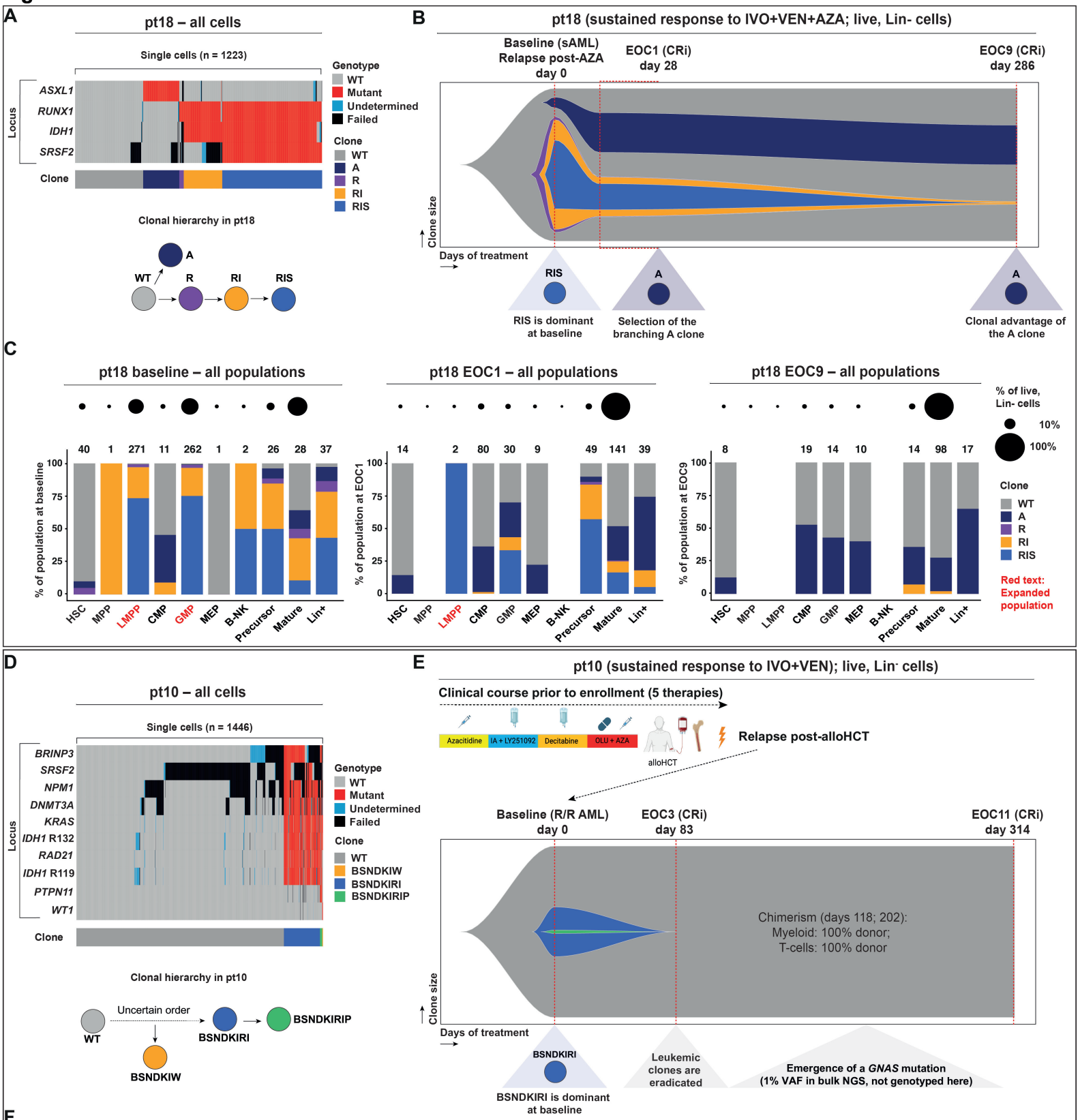
A
pt18 – all cells
Single cells (n = 1223)
Locus
ASXL1
RUNX1
IDH1
SRSF2
Clone
Genotype
WT
Mutant
Undetermined
Failed
Clone
WT
A
R
RI
RIS
Clonal hierarchy in pt18
WT
A
R
RI
RIS
B
pt18 (sustained response to IVO+VEN+AZA; live, Lin- cells)
Baseline (sAML)
Relapse post-AZA
day 0
EOC1 (CRi)
day 28
EOC9 (CRi)
day 286
Clone size
Days of treatment
RIS
RIS is dominant at baseline
A
Selection of the branching A clone
A
Clonal advantage of the A clone
C
pt18 baseline – all populations
pt18 EOC1 – all populations
pt18 EOC9 – all populations
% of live, Lin- cells
10%
100%
% of population at baseline
% of population at EOC1
% of population at EOC9
40 1 271 11 262 1 2 26 28 37
14 2 80 30 9 49 141 39
8 19 14 10 14 98 17
HSC MPP LMPP CMP GMP MEP B-NK Precursor Mature Lin+
Clone
WT
A
R
RI
RIS
Red text: Expanded population
D
pt10 – all cells
Single cells (n = 1446)
Locus
BRINP3
SRSF2
NPM1
DNMT3A
KRAS
IDH1 R132
RAD21
IDH1 R119
PTPN11
WT1
Clone
Genotype
WT
Mutant
Undetermined
Failed
Clone
WT
BSNDKIW
BSNDKIRI
BSNDKIRIP
Clonal hierarchy in pt10
Uncertain order
WT
BSNDKIRI
BSNDKIRIP
BSNDKIW
E
pt10 (sustained response to IVO+VEN); live, Lin- cells
Clinical course prior to enrollment (5 therapies)
Azacitidine
IA + LY251092
Decitabine
OLU + AZA
alloHCT
Relapse post-alloHCT
Baseline (R/R AML)
day 0
EOC3 (CRi)
day 83
EOC11 (CRi)
day 314
Chimerism (days 118; 202):
Myeloid: 100% donor;
T-cells: 100% donor
Clone size
Days of treatment
BSNDKIRI
BSNDKIRI is dominant at baseline
Leukemic clones are eradicated
Emergence of a GNAS mutation
(1% VAF in bulk NGS, not genotyped here)
F
pt10 baseline – all populations
pt10 EOC3 – all populations
pt10 EOC11 – all populations
% of live, Lin- cells
10%
100%
% of population at baseline
% of population at EOC3
% of population at EOC11
4 201 85 84
2 9 12 6 3 51 193 155
4 1 24 72 28 20 140 128 224
HSC MPP LMPP MLP CMP GMP MEP B-NKp Precursor Mature Lin+
Clone
WT
BSNDKIW
BSNDKIRI
BSNDKIRIP
Red text: Expanded population

Figure 6

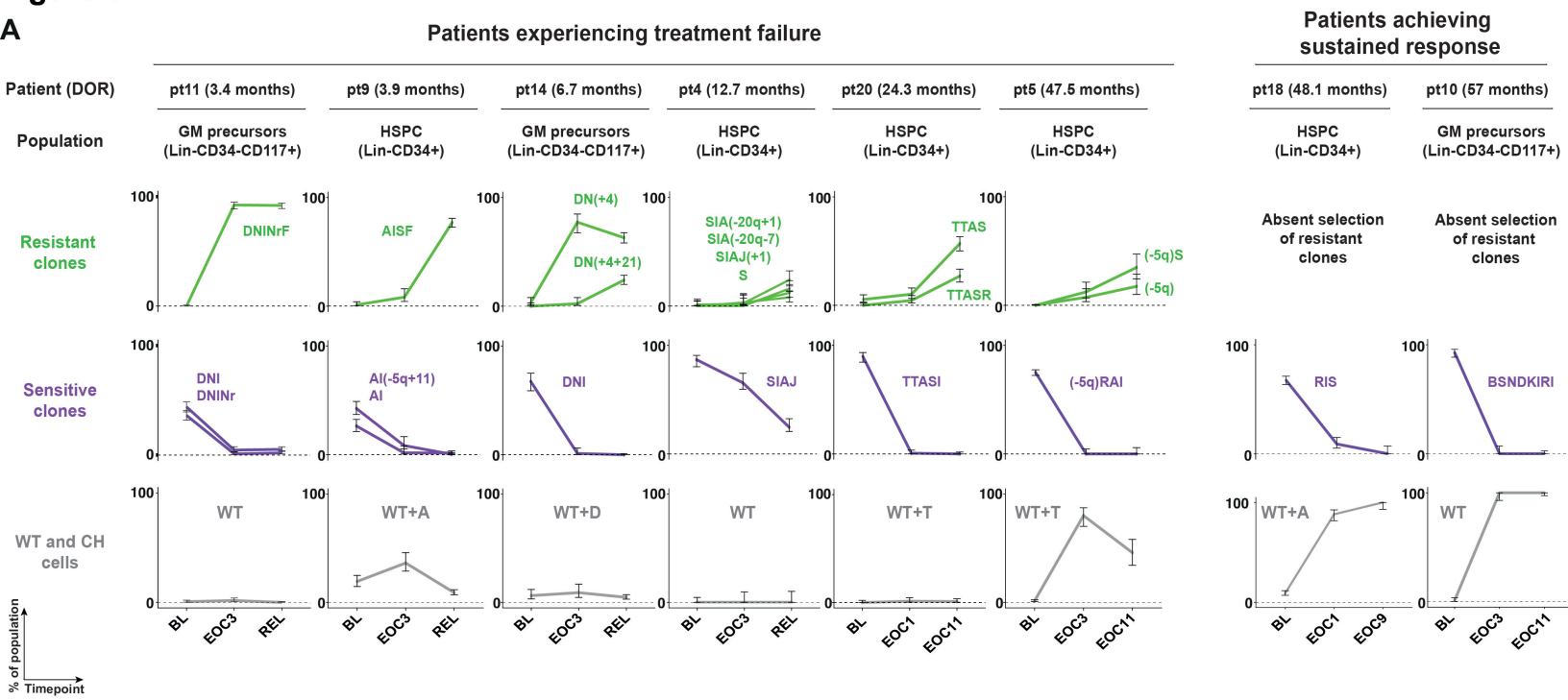
A
Patients experiencing treatment failure
Patients achieving sustained response
Patient (DOR)
pt11 (3.4 months)
pt9 (3.9 months)
pt14 (6.7 months)
pt4 (12.7 months)
pt20 (24.3 months)
pt5 (47.5 months)
pt18 (48.1 months)
pt10 (57 months)
Population
GM precursors (Lin-CD34-CD117+)
HSPC (Lin-CD34+)
GM precursors (Lin-CD34-CD117+)
HSPC (Lin-CD34+)
HSPC (Lin-CD34+)
HSPC (Lin-CD34+)
HSPC (Lin-CD34+)
GM precursors (Lin-CD34-CD117+)
Resistant clones
DNINrF
AISF
DN(+4)
DN(+4+21)
SIA(-20q+1)
SIA(-20q-7)
SIAJ(+1)
S
TTAS
TTASR
(-5q)S
(-5q)
Absent selection of resistant clones
Absent selection of resistant clones
Sensitive clones
DNI
DNINr
AI(-5q+11)
AI
DNI
SIAJ
TTASI
(-5q)RAI
RIS
BSNDKIRI
WT and CH cells
WT
WT+A
WT+D
WT
WT+T
WT+T
WT+A
WT
BL
EOC3
REL
EOC1
EOC11
EOC9
100
0
% of population
Timepoint

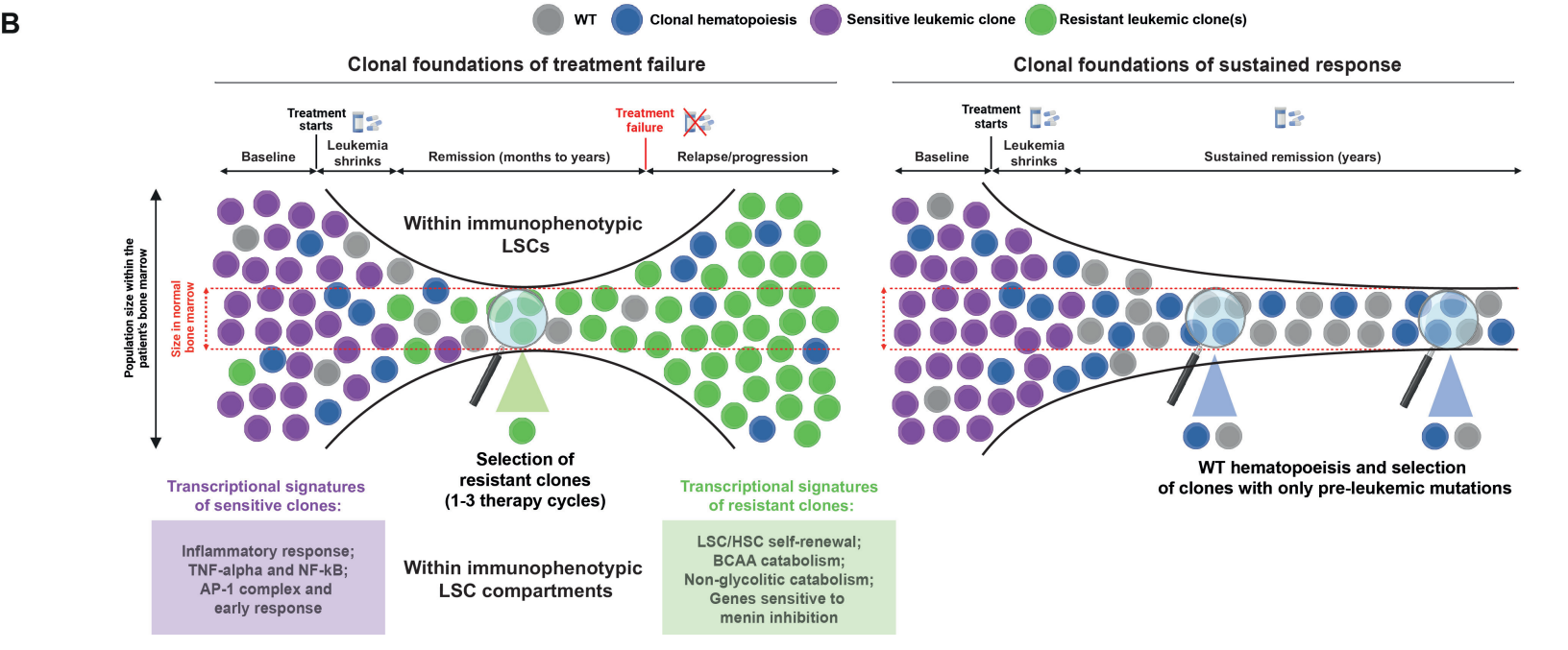
B
WT
Clonal hematopoiesis
Sensitive leukemic clone
Resistant leukemic clone(s)
Clonal foundations of treatment failure
Clonal foundations of sustained response
Treatment starts
Treatment failure
Baseline
Leukemia shrinks
Remission (months to years)
Relapse/progression
Sustained remission (years)
Population size within the patient's bone marrow
Size in normal bone marrow
Within immunophenotypic LSCs
Selection of resistant clones (1-3 therapy cycles)
WT hematopoeisis and selection of clones with only pre-leukemic mutations
Transcriptional signatures of sensitive clones:
Inflammatory response; TNF-alpha and NF-kB; AP-1 complex and early response
Within immunophenotypic LSC compartments
Transcriptional signatures of resistant clones:
LSC/HSC self-renewal; BCAA catabolism; Non-glycolitic catabolism; Genes sensitive to menin inhibition

Clonal and transcriptional basis of resistance and response to ivosidenib combination therapies in *IDH1*-mutated myeloid malignancies

Context of Research

In a Phase Ib/II clinical trial, ivosidenib + venetoclax ± azacitidine have demonstrated encouraging clinical activity in *IDH1*-mutated patients. However, 29% of patients relapsed.

Aim of This Study

Through simultaneous single-cell genotyping and RNA-seq on index-sorted single cells, we studied longitudinal dynamics of clonal response and transcriptional features of relapse.

Findings

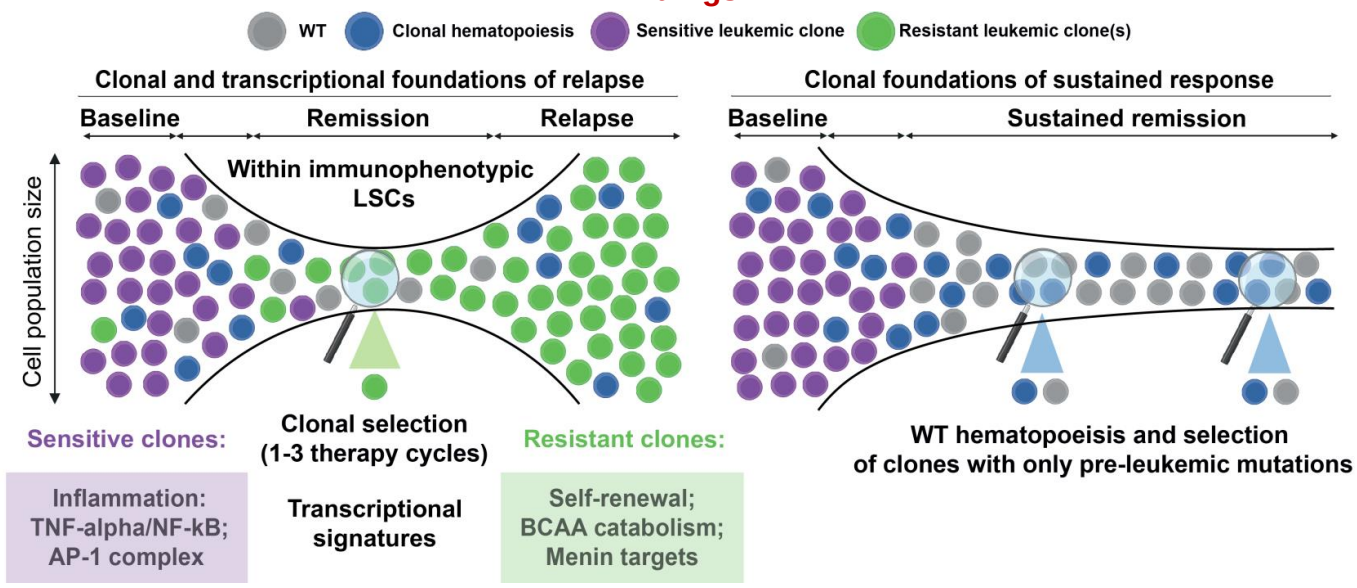

Conclusions: **Clonal selection associated with relapse or eradication of leukemic clones associated with durable response occur rapidly, during 1-3 therapy cycles. Resistant clones upregulate transcriptional signatures of LSC/HSC self-renewal, branched-chain amino acid catabolism, and menin targets.**

*Turkalj et al. DOI: 10.xxxx/**blood**.2025xxxxxx*